

# SMC Bulletin

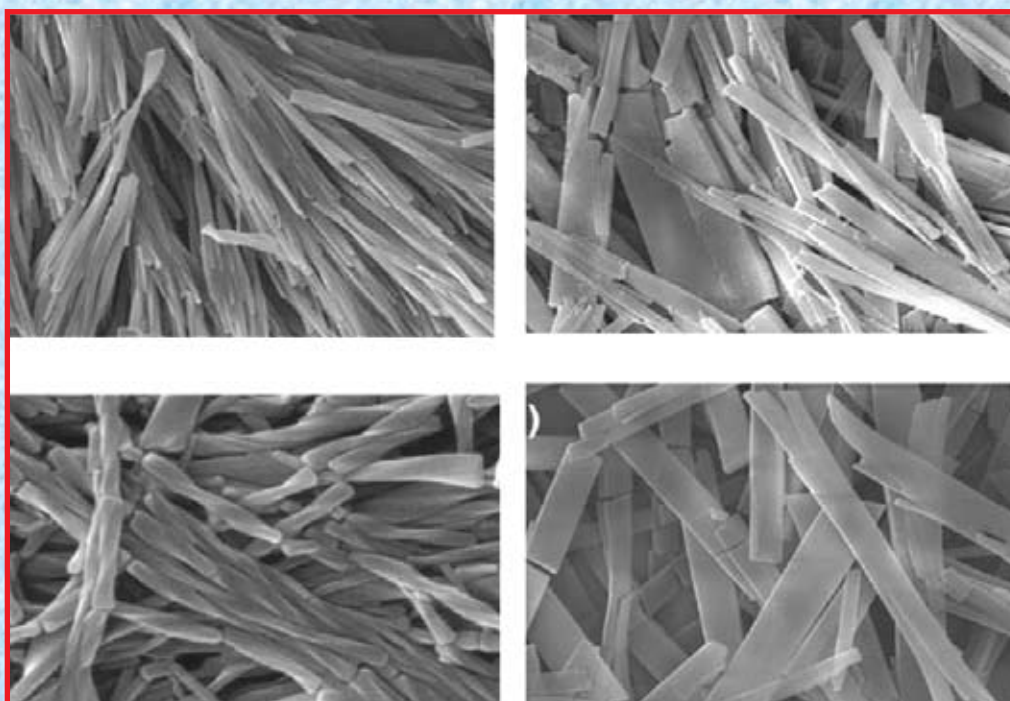
ISSN 2394-5087

A Publication of the Society for Materials Chemistry

Volume 9

No. 1

April 2018



**Special Issue on Energy and Bio Materials**



# Society for Materials Chemistry

Society for Materials Chemistry was mooted in 2007 with following aims and objectives:

- (a) to help the advancement, dissemination and application of the knowledge in the field of materials chemistry,
- (b) to promote active interaction among all material scientists, bodies, institutions and industries interested in achieving the advancement, dissemination and application of the knowledge of materials chemistry,
- (c) to disseminate information in the field of materials chemistry by publication of bulletins, reports, newsletters, journals.
- (d) to provide a common platform to young researchers and active scientists by arranging seminars, lectures, workshops, conferences on current research topics in the area of materials chemistry,
- (e) to provide financial and other assistance to needy deserving researchers for participation to present their work in symposia, conference, etc.
- (f) to provide an incentive by way of cash awards to researchers for best thesis, best paper published in journal/national/international conferences for the advancement of materials chemistry,
- (g) to undertake and execute all other acts as mentioned in the constitution of SMC.

## Executive Committee

### President

**Dr. V. K. Jain**

Bhabha Atomic Research Centre  
Trombay, Mumbai, 400 085  
[jainvk@barc.gov.in](mailto:jainvk@barc.gov.in)

### Vice-Presidents

**Dr. A. K. Tyagi**

Bhabha Atomic Research Centre  
Trombay, Mumbai, 400 085  
[jainvk@barc.gov.in](mailto:jainvk@barc.gov.in)

**Dr. C. S. Sundar**

J.C. Bose Fellow & Sr. Professor,  
HBNI Materials Science Group  
Indira Gandhi Centre for Atomic  
Research Kalpakkam, 603102  
[css@igcar.gov.in](mailto:css@igcar.gov.in)

### Secretary

**Dr. P. A. Hassan**

Bhabha Atomic Research Centre  
Trombay, Mumbai, 400 085  
[hassan@barc.gov.in](mailto:hassan@barc.gov.in)

### Treasurer

**Dr. Sandeep Nigam**

Bhabha Atomic Research Centre  
Trombay, Mumbai, 400 085  
[snigam@barc.gov.in](mailto:snigam@barc.gov.in)

### Members

**Dr. K. C. Barick**  
Bhabha Atomic Research Centre  
Trombay, Mumbai-400085

**Dr. S. Kannan**

Bhabha Atomic Research Centre  
Trombay, Mumbai-400085

**Shri. R. K. Mishra**

Bhabha Atomic Research Centre  
Trombay, Mumbai-400085

**Dr. Ratikant Mishra**

Bhabha Atomic Research Centre  
Trombay, Mumbai-400085

**Dr. G. Mugesh**

Indian Institute of Science  
Bangalore-560012

**Dr. (Smt.) Mrinal Pai**

Bhabha Atomic Research Centre  
Trombay, Mumbai-400085

**Dr. Vivek Polshettiwar**

Tata Institute Atomic Research Centre  
Colaba, Mumbai-400005

**Dr. S. K. Sarkar**

Raja Ramanna Fellow  
Bhabha Atomic Research Centre  
Trombay, Mumbai-400085

**Dr. A. K. Tripathi**

Bhabha Atomic Research Centre  
Trombay, Mumbai-400085

**Dr. R. K. Vatsa**

Bhabha Atomic Research Centre  
Trombay, Mumbai-400085

**Dr. V. Venugopal**

Raja Ramanna Fellow  
Bhabha Atomic Research Centre  
Trombay, Mumbai-400085

### Co-opted Members

**Prof. Anshu Dandia**

University of Rajasthan  
Jaipur-302004

**Dr. D. Das**

Raja Ramanna Fellow  
Bhabha Atomic Research Centre  
Trombay, Mumbai-400085

**Prof. A. K. Ganguli**

Institute of Nano Science  
and Technology  
Mohali, Punjab - 160062

**Dr. K. M. Parida**

Institute of Technical Education  
& Research  
Siksha 'O' Anusandhan University  
Bhubaneswar-751030

**Dr. V. Sudarsan**

Bhabha Atomic Research Centre  
Trombay, Mumbai-400085

---

Contact address

**Society for Materials Chemistry**

C/o Chemistry Division

Bhabha Atomic Research Centre, Trombay, Mumbai, 400 085, India

Tel: +91-22-25592001, E-mail: [socmatchem@gmail.com](mailto:socmatchem@gmail.com)

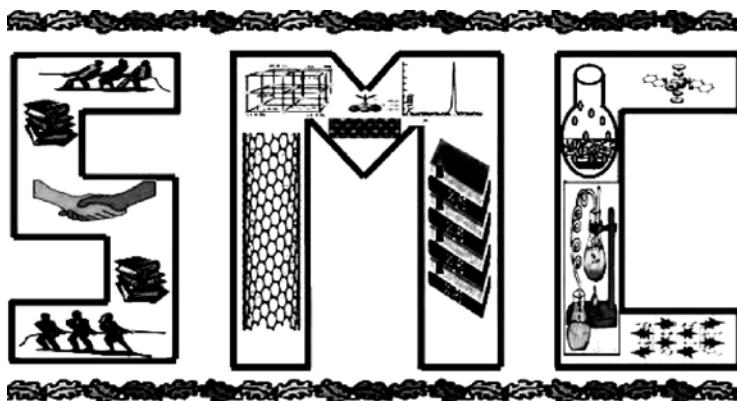
# SMC Bulletin

A Publication of the Society for Materials Chemistry

Volume 9

No. 1

April 2018



SOCIETY FOR MATERIALS CHEMISTRY

# SMC Bulletin

Vol. 9

Nos. 1

April 2018

## Guest Editor

**Prof. Neeraj Agarwal**

UM-DAE Centre for Excellence in Basic Sciences  
University of Mumbai, Kalina,  
Santacruz (E), Mumbai 400 098

Editorial Board	
<b>Dr. Arvind Kumar Tripathi</b> Chemistry Division Bhabha Atomic Research Centre Trombay, Mumbai, 400 085 e-mail: catal@barc.gov.in	
<b>Dr. Manidipa Basu</b> Chemistry Division Bhabha Atomic Research Centre Trombay, Mumbai, 400 085 e-mail: deepa@barc.gov.in	<b>Dr. Rajesh Ganesan</b> Materials Chemistry Division Indira Gandhi Centre for Atomic Research, Kalpakkam, 603102 e-mail: rajesh@igcar.gov.in
<b>Dr. G. Kedarnath</b> Chemistry Division Bhabha Atomic Research Centre Trombay, Mumbai, 400 085 e-mail: deepa@barc.gov.in	<b>Dr. Sandeep Nigam</b> Chemistry Division Bhabha Atomic Research Centre Trombay, Mumbai, 400 085 e-mail: snigam@barc.gov.in
<b>Dr. Rajesh V. Pai</b> Fuel Chemistry Division Bhabha Atomic Research Centre Trombay, Mumbai, 400 085 e-mail: rajeshvp@barc.gov.in	<b>Dr. Vivek Polshettiwar</b> Department of Chemical Sciences, Tata Institute of Fundamental Research, Colaba, Mumbai 400005 e-mail: vivekpol@tifr.res.in

---

## Published by

Society for Materials Chemistry  
C/o. Chemistry Division  
Bhabha Atomic Research Centre, Trombay, Mumbai, 400 085  
E-mail: socmatchem@gmail.com, Tel: +91-22-25592001

*Please note that the authors of the paper are alone responsible for the technical contents of papers and references cited therein.  
Front cover shows self-assembly of benzothiazole derivative (TTBT) in different solvents*

---

---

## Guest Editorial

---

---



**Neeraj Agarwal**

Materials are integral components in numerous energy and bio applications. Development of materials for alternative energy sources is a major challenge to materials scientists today. Organic and inorganic molecules have recently shown potential for their wide application in sustainable and green energy sources.

The focus of this issue of SMC bulletin is on the synthesis and characterization of different types of materials and their applications in energy and bio-medical areas. In this issue, articles are covering the topics such as materials and characterization of fluorescent nano-materials, materials for solar hydrogen generation, conducting nano-composites of organic-inorganic hybrids. Also, novel biomaterials to study the complete elimination of tumour cells, epigenetic assays for developing algae for screening of cancer drugs are discussed. Couple of articles are on the role of albumin nano-particles on drug delivery and effect of antioxidants on albumin aggregation.

It has been a pleasure to act as guest editor for this special issue on "*Energy and Biomaterials*". I thank Prof. V. K. Jain, President, SMC and editorial board of SMC bulletin for this opportunity. I also thank all the authors who agreed for contributing articles for this issue.

I hope that the readers will find the articles informative and useful.



---

---

## From the desks of the President and Secretary

---

---



**Dr. V.K. Jain**  
*President*



**Dr. P. A. Hassan**  
*Secretary*

Dear Fellow Members and Readers,  
Greetings from the Executive Council of SMC

Since its inception, SMC has been regularly updating its members with advances in the area of materials chemistry, by way of publishing articles in SMC Bulletin and organising workshops/symposia, etc. This provides ample opportunity for researchers/ academicians and industrial partners to discuss and share recent developments in specific areas. With this objective, in December 2017, SMC conducted its flagship workshop, NWMC-2017 at UM-DAE Centre for Excellence in Basic Sciences, University of Mumbai, Santacruz (E) Mumbai. We are happy to let you know that the workshop was a great success with more than 150 participants from various Institutes. The theme of the 4th NWMC-2017 was Energy and Biomaterials (abbreviated as NWMC- ENBIO-MAT) and deliberations during this workshop became the genesis for bringing out this issue.

The demand for energy consumption is ever increasing and is expected to be alarming for developing countries. Increased per capita consumption of electricity warrants exploration of advanced materials and technologies for green and sustainable energy production. Materials development to harness all possible sources of energy in an efficient manner is of paramount importance. Another important program that has gained momentum in recent years is providing affordable healthcare to the mankind. Research related to both energy and healthcare materials were discussed during 4th NWMC-2017. In this issue, we bring together a compendium of different articles relevant to energy materials and biomaterials research in India. Controlling the architecture of donor-acceptor complexes and aggregation induced photo-physical processes go a long way in designing efficient energy conversion materials. Modulating electrical properties of conducting polymers via inorganic-organic composites offers excellent way to alter its electrical behaviour. In the area of biomaterials, research is underway to develop novel assays to track epigenetic memories in model systems, developing efficient ways to prevent protein aggregation induced diseases, and in development of new drug delivery vehicles and so on.

We would like to put on record our sincere appreciation to Dr. Neeraj Agarwal- the Guest Editor, who was also the convenor of NWMC-2017, for his interest and all the authors for contributing an article to this special issue. We are indebted to all our members and readers for their constant endeavour to support the growth of the Society.



# CONTENTS

Feature article	Page No.
1 <b>Fluorescent nanoaggregates through molecular self-assembly: morphology control and spectroscopic investigation</b> <i>MD. Waseem Hussain and Abhijit Patra</i>	1
2 <b>Influence of particle size of albumin nanoparticles on its drug loading and cellular uptake</b> <i>Beena G. Singh, Ram P. Das, Amit Kunwar</i>	8
3 <b>Effect of Zinc Oxide Nanoparticles on dc Electrical Conductivity of Inorganic-Organic Conducting Nanocomposites</b> <i>Shahid Pervez Ansari and Faiz Mohammad</i>	13
4 <b>Strategic design of gold nanoparticles for the complete elimination of tumour cells: Potential and challenges</b> <i>Manu Lopus</i>	20
5 <b>Effects of antioxidants melatonin and glutathione on human serum albumin aggregation: biophysical studies</b> <i>Vikas Kumar, Ramakrishna V. Hosur and Sinjan Choudhary</i>	22
6 <b>Exploiting Materials to Design Novel Epigenetic Assays Towards Developing Algae for Screening Cancer Drugs</b> <i>Subhojit Sen, Pooja Potdar and Patricia Pinto</i>	29
7 <b>Plasmonic modification of NaNbO<sub>3</sub>-CdS heterostructure photocatalyst for enhanced solar hydrogen generation</b> <i>Kamala K. Nanda, Hardik Jain, Smrutirekha Swain and Yatendra S. Chaudhary</i>	33



# Fluorescent nanoaggregates through molecular self-assembly: morphology control and spectroscopic investigation

MD. Waseem Hussain\* and Abhijit Patra\*

Department of Chemistry, Indian Institute of Science Education and Research Bhopal, Bhopal Bypass Road, Bhauri, Bhopal 462066, Madhya Pradesh, India

E-mail: waseemh@iiserb.ac.in, abhijit@iiserb.ac.in

## Abstract

A new organic fluorophore involving donor-acceptor units was fabricated. Tetraphenylethene which exhibits strong fluorescence in the aggregated state was used as a donor and benzo[c][1,2,5]thiadiazole was employed as an acceptor. The donor and acceptor are linked through a  $\pi$ -linker involving triazole unit. The coupled product, TTBT showed enhanced emission in the solution as well as in the solid state. The specific solvent effect on the fluorescence properties of TTBT was observed in DMSO which could be due to the intramolecular charge transfer characteristics. Remarkably, TTBT spontaneously self-assembled to size and shape-tunable nanostructures by fine-tuning of the solvent environments. The morphological studies of TTBT in various polar solvents showed twisted nanostructures whereas, predominantly in the aqueous medium showed planar one-dimensional (1D) assemblies. The interesting case of helical nanostructures was observed in pure *N,N*-dimethylformamide (DMF). The present study demonstrates that the understanding of molecular self-assembly process leads to the fabrication of well-defined fluorescent nanostructures like nanorods, nanohelices, nanobelts and nanoparticles.

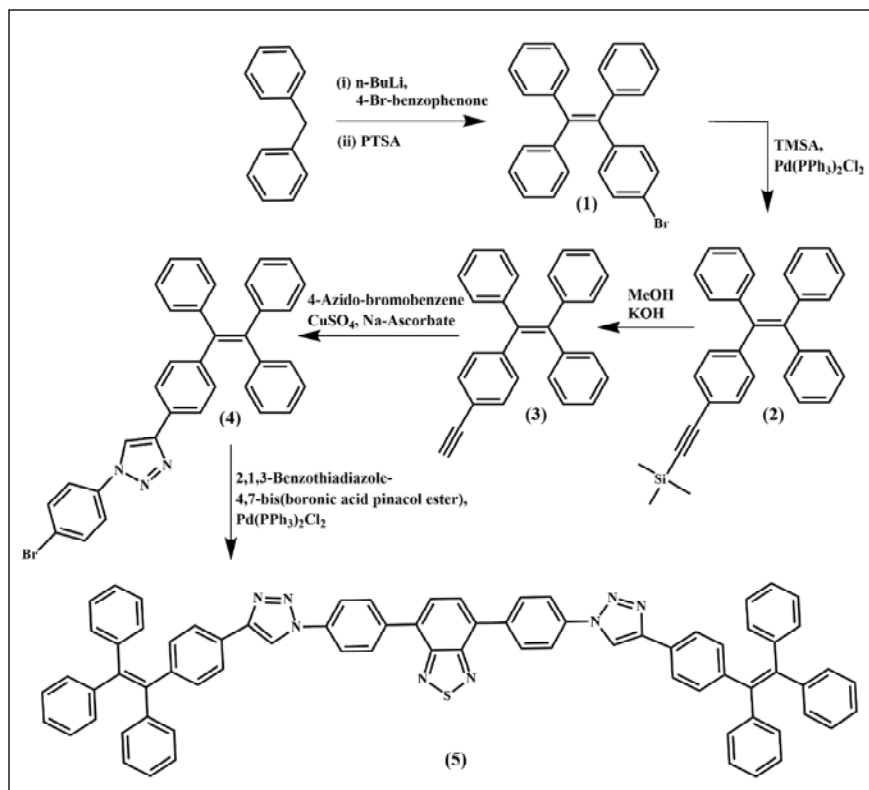
## Introduction

Fluorescent molecular nanomaterials especially those based on small molecules have received significant attention due to their wide-ranging application potential. However, the development of a simple strategy to fabricate size and shape-tunable molecular nanostructure and understanding the structure-property relationship is a great challenge. The “top-down” strategy which is extensively used for producing inorganic nanostructures is often difficult to apply to most of the organic materials due to the thermal instability of the latter. In this context, molecular self-assembly has been emerged as a convenient strategy to fabricate organic nanostructures.<sup>1,2</sup> It involves the spontaneous organization of molecules mostly under thermodynamic equilibrium conditions into structurally well-defined and stable arrangements. The fine-tuning of weak, noncovalent interactions like dipole-dipole, ion-dipole, H-bonding, electrostatic and dispersion interactions play a major role in controlling the molecular self-assembly processes.<sup>1,3</sup> The design principle of the molecules and supramolecular entities with specific shape and architecture leading to the aggregation into desired structures is the key issue here.

Some of the landmark examples of molecular assemblies leading to hierarchical nanostructures include microcapsules,<sup>4</sup> vesicles,<sup>5</sup> liposomes,<sup>6</sup> micelles,<sup>7</sup> dendrimers,<sup>8</sup> gels,<sup>9</sup> etc. A rich variety of nanostructures have been fabricated through self-assembly of molecules in solutions.<sup>3,10-12</sup> Organic nanotubes and nanofibers were

reported based on long-chain amphiphilic molecules.<sup>3,12</sup> Numerous 1D nanostructures of different derivatives of perylene-3,4,9,10-tetracarboxylicdiimide (PTCDI) and hexa-peri-hexabenzocoronene (HBC) were fabricated through self-assembly in solution phase.<sup>10,11</sup> Self-assembly of conjugated molecules into 1D structures has potential applications in photonics and optoelectronics<sup>13</sup> such as, organic light emitting diodes (OLEDs), field-effect transistors (FETs), and solar cells.<sup>14-22</sup> The performance of the optoelectronic devices highly relies on the intermolecular interactions and the molecular ordering in the assemblies. Hence, it is important to develop a novel class of fluorophores capable of forming spontaneous self-assembled nanostructures of demand with enhanced solid-state optical properties.

Herein, we report the synthesis, self-assembly and photophysical properties of tetraphenylethene, triazole and benzothiadiazole based fluorophoric system 4,7-bis(4-(4-(1,2,2-triphenylvinyl)phenyl)-1H-1,2,3-triazol-1-yl)phenyl)benzo[c][1,2,5]thiadiazole (TTBT). TTBT exhibits strong fluorescence both in solution as well as in the solid state. The fine tuning of the good solvent and anti-solvent mixture led to a spontaneous assembly of TTBT into the nanorods, nanofibers as well as the rectangular nanosheets at room temperature. Moreover, these nanofibers are twisted and even found to be helical though they are devoid of any chiral centers. The self-assembly of TTBT was explored through spectroscopic and microscopic investigations.



**Scheme 1:** Synthetic route to tetraphenylethylene-triazole-benzothiadiazole-based compound, TTBT.

## Materials and methods:

Diphenylmethane (99%), *n*-butyllithium (2.0 M) in cyclohexane, copper(I) iodide (99.995%), bis(triphenylphosphine)palladium(II) dichloride (98%), 2,1,3-benzothiadiazole-4,7-bis(boronic acid pinacol ester) (95%), (+)-sodium L-ascorbate (>98%), copper(II) sulfate pentahydrate (>98%), 4-bromoaniline (97%), ethynyltrimethylsilane (98%), sodium azide (>99.5%), 4-bromobenzophenone (98%), triphenylphosphine (>98.5%), potassium phosphate tribasic (>98%) were received from Sigma-Aldrich. Sodium nitrite (>98%), dichloromethane chloroform and hexane were received from Merck. THF (99%), ethanol (99.8%), extra pure concentrated HCl were received from Spectrochem. 1,4-Dioxane was received from SD fine-Chem Limited.

<sup>1</sup>H and <sup>13</sup>C-NMR spectra were recorded on Bruker Avance III 500 MHz NMR spectrometers. The chemical shifts ( $\delta$ ) are reported in parts per million (ppm) using residual solvent signals as internal standards. MALDI spectra were recorded using Bruker Daltonics flexAnalysis; the instrument type used was ultraflexTOF (Time of Flight). The morphological studies were carried out using a Carl Zeiss (Ultraplus) field emission scanning electron microscope. Samples for microscopy were prepared by drop-casting  $\sim 10 \mu\text{L}$  of the solution over a silicon

wafer, glued to the aluminium stub using adhesive carbon tape. All samples were coated with a thin layer of sputtered gold prior to imaging. FESEM was carried out using an accelerating voltage of 5 kV and 10 kV. UV-Visible absorption spectra were recorded on Cary 100 spectrophotometer using 10 mm path length quartz cuvette. All the steady-state fluorescence measurements were carried out on JobinYvon Horiba Model Fluorolog-3-21 using 10 mm quartz cuvette.

## Synthesis of TTBT:

### Synthesis of (2-(4-bromophenyl)ethene-1,1,2-triyl)tribenzene (1):

(1) was synthesized following a reported procedure.<sup>23</sup> To diphenylmethane (2.0 g, 12 mmol) in dry tetrahydrofuran (15 mL), 5 mL of a 2 M solution of *n*-butyllithium in hexane (10 mmol) was added at 0 °C under nitrogen atmosphere. The stirring was continued for 30 min at 0 °C. The above mixture was added with 4-bromobenzophenone (9 mmol) and the temperature was increased to room temperature slowly and further

stirred for 6 h. The reaction was quenched with ammonium chloride solution and the organic layer was extracted with dichloromethane (200 mL). The organic layer was dried over MgSO<sub>4</sub> and was evaporated and subsequently was subjected to acid-catalyzed dehydration. The crude alcohol was dissolved in 80 mL of toluene in a 250 mL Schlenk flask fitted with a Dean-Stark apparatus. A catalytic amount of *p*-toluenesulphonic acid (342 mg, 1.8 mmol) was added and the mixture was refluxed for 3–4 h and cooled to room temperature. The toluene layer was washed with 10% aqueous NaHCO<sub>3</sub> solution (150 mL) and dried over anhydrous MgSO<sub>4</sub> and evaporated to obtain the crude tetraphenylethylene derivative. The crude product was purified by column chromatography using hexane as eluent to obtain the product with 90% yield. <sup>1</sup>H NMR:  $\delta_{\text{H}}$  (500 MHz, CDCl<sub>3</sub>) 7.23–7.22 (2H, d), 7.15–7.09 (9H, m), 7.04–7.00 (6H, m), 6.91–6.89 (2H, d).

### Synthesis of trimethyl((4-(1,2,2-triphenylvinyl)phenyl)ethynyl) silane (2):

Into a 25 mL round-bottom flask, Pd(PPh<sub>3</sub>)<sub>2</sub>Cl<sub>2</sub> (12 mg, 0.017 mmol), CuI (5 mg, 0.026 mmol), PPh<sub>3</sub> (10 mg, 0.04 mmol), **1** (250 mg, 0.61 mmol), and a mixture of THF/TEA/piperidine (7:6:1 v/v/v) (14 mL) were added under nitrogen. After the catalysts and the starting materials were completely dissolved, trimethylsilylacetylene (75 mg,

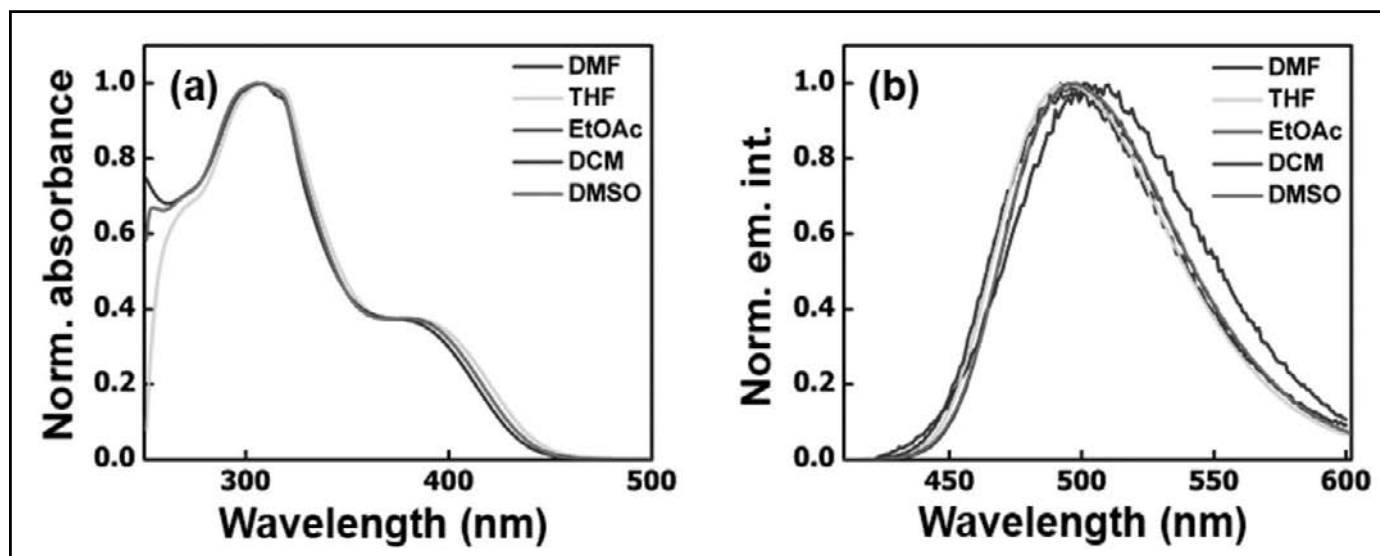


Figure 1(a) Normalized absorption and (b) normalized emission spectra of TTBT in DMF, THF, EtOAc, DCM and DMSO.

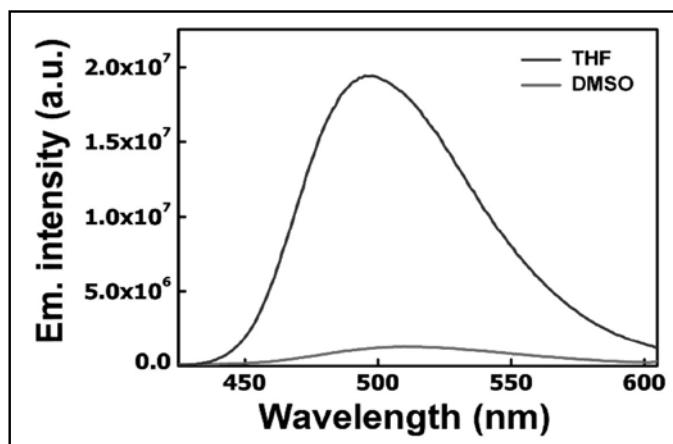


Figure 2 The relative fluorescence intensity of TTBT in THF and DMSO.

0.72mmol) was injected into the flask and then was stirred at 55 °C for 24 h. After the reaction, the mixture was filtered and the solid was washed with diethyl ether. The filtrate was concentrated by a rotary evaporator and the crude product was purified by a silica gel column chromatography using 5% DCM/hexane mixture as eluent. The pale yellow solid of **2** was obtained in 84% yield.  $^1\text{H}$  NMR:  $\delta_{\text{H}}$ (500 MHz,  $\text{CDCl}_3$ ) 7.21-7.20 (2H, d), 7.13-7.09 (9H, m), 7.03-6.99 (6H, m), 6.97-6.95 (2H, m), 0.22 (9H, s).

#### Synthesis of 1-(4-ethynylphenyl)-1,2,2-triphenylethene (**3**):

**2** (200 mg, 0.46 mmol) and dry THF (25 mL) were taken in a 100 mL round-bottom flask. Later TBAF (240 mg, 0.92 mmol) was added and stirred at RT for 12 h. After the reaction, the solvent was removed by rotary evaporator and the crude product was purified by column chromatography using 10% DCM/hexane mixture as eluent. The pale yellow

solid of **3** was obtained in 92% yield.  $^1\text{H}$  NMR:  $\delta_{\text{H}}$ (500 MHz,  $\text{CDCl}_3$ ) 7.24-7.22 (2H, d), 7.13-7.09 (9H, m), 7.04-7.00 (6H, m), 6.98 (2H, d), 3.03 (1H, s).

#### Synthesis of 1-(4-bromophenyl)-4-(4-(1,2,2-triphenylvinyl)phenyl)-1H-1,2,3-triazole (**4**):

Into a 25 mL Schlenk tube, **3** (0.28 mmol) and 4-bromoazidobenzene (0.28 mmol) were added and then evacuated and refilled with argon for three times. Dry THF (10 mL) and triethylamine (1 mL) were added under an argon atmosphere. After the dissolution of the monomers, the reaction mixture was added with freshly prepared aq. solution of sodium ascorbate (1 M, 28  $\mu\text{L}$ ) and  $\text{CuSO}_4$  (1 M, 14  $\mu\text{L}$ ) under an inert atmosphere. The reaction was stirred at 70 °C for 6 h. After bringing it to room temperature, the reaction mixture was added to 80 mL of distilled water and extracted with DCM. The organic layers were combined and dried over anhydrous  $\text{Na}_2\text{SO}_4$ . The solvent was evaporated and the obtained coupled product was subjected to silica-gel column chromatography using 60% DCM/hexane as eluent. An off-white solid was collected with a yield of 95%.  $^1\text{H}$  NMR:  $\delta_{\text{H}}$ (500 MHz,  $\text{CDCl}_3$ ) 8.09 (1H, s), 7.66 (4H, s), 7.64-7.63 (2H, d), 7.13-7.03 (17H, m).  $^{13}\text{C}$  NMR:  $\delta$  (126 MHz,  $\text{CDCl}_3$ ) 143.59, 143.48, 132.95, 131.97, 131.39, 131.32, 127.81, 127.75, 127.67, 126.58, 126.53, 125.18, 121.84, 120.74, 119.6, 117.22. MS (MALDI-TOF): calc. 554.49. Found 554.20.

#### Synthesis of 4,7-bis(4-(4-(1,2,2-triphenylvinyl)phenyl)-1H-1,2,3-triazol-1-yl)phenyl)benzo[c][1,2,5]thiadiazole (**5**):

**4** (0.198 mmol), 4,7-bis(4,4,5,5-tetramethyl-1,3,2-dioxaborolan-2-yl)benzo[c][1,2,5]thiadiazole (0.09 mmol),



Figure 3 Self-assembly of TTBT in different solvent environments:(a) the aqueous dispersion of nanoparticles obtained by the reprecipitation method, (b) 1D nanorods in THF/water mixture and (c) 1D nanorods in THF/MeOH mixture.

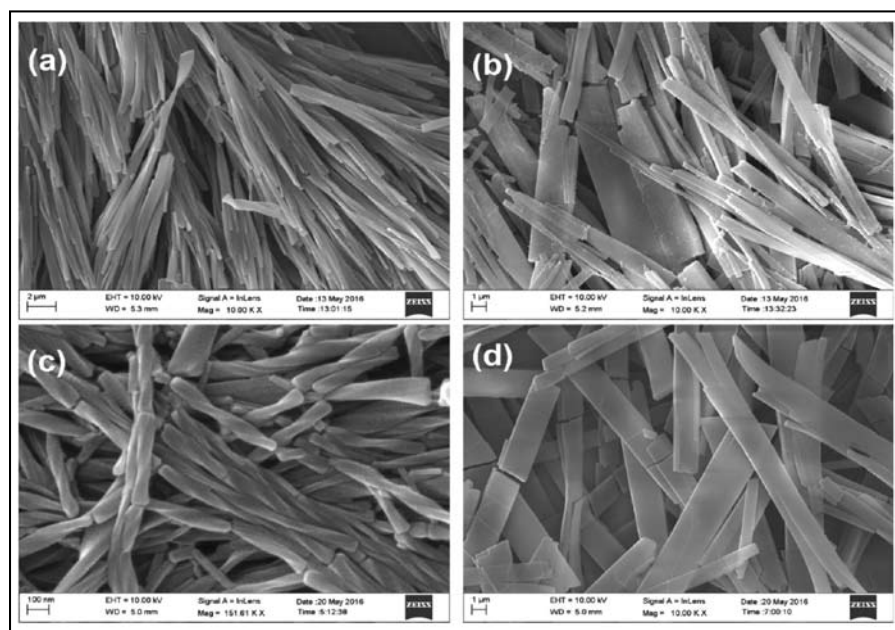


Figure 4 Self-assembly of TTBT in different solvents: (a) DMSO, (b) DMSO/water (2:1), (c) DMF and (d) DMF/water (2:1).

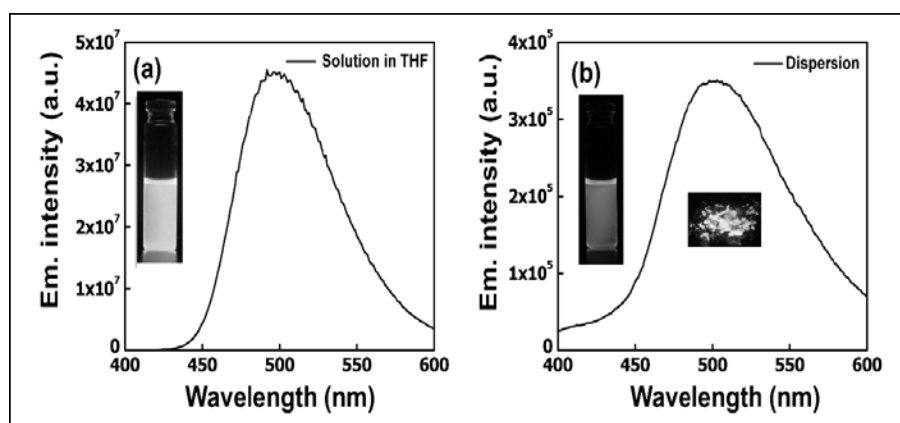


Figure 5 The fluorescence emission spectra of TTBT in (a) solution (THF) and (b) aqueous dispersion of nanoparticles. Inset: the respective photographs of TTBT in solution, nanoparticles and solid state under irradiation of 365 nm UV light depicting strong fluorescence.

Pd(PPh<sub>3</sub>)<sub>4</sub> (0.004 mmol) were added in a 25 mL Schlenk tube. The reaction vessel was evacuated and then filled with argon for three times. 2 M K<sub>2</sub>CO<sub>3</sub> aqueous solution was added to it, followed by the degassed 2:1 mixture of THF/water (7.5 mL). The reaction mixture was stirred at 80 °C for 24 h. Subsequently, the reaction mixture was quenched with distilled water and then extracted with DCM. The crude product was subjected to silica-gel column chromatography using 60% DCM/hexane as eluent. A green color solid was obtained with a yield of 64%. <sup>1</sup>H NMR: δ<sub>H</sub> (500 MHz, CDCl<sub>3</sub>) 8.21 (2 H, s), 8.20-8.18 (4 H, d), 7.98-7.97 (4 H, d), 7.90 (2H, s), 7.70-7.68 (4H, d), 7.16-7.04 (34H, m). <sup>13</sup>C NMR: δ (126 MHz, CDCl<sub>3</sub>) 153.91, 148.48, 143.62, 143.52, 141.49, 140.41, 137.59, 136.93, 136.88, 131.99, 131.41, 131.37, 131.34, 130.84, 130.66, 128.26, 128.23, 128.07, 127.83, 127.76, 127.68, 126.62, 126.59, 126.54, 125.22, 120.53, 117.29. MS (MALDI-TOF): calc. 1083.33. Found 1083.60.

### Sample preparation for morphological studies:

The nanoassemblies were prepared by layering the anti-solvent over the solution of TTBT in the particular solvent of interest. The overall concentration of TTBT was kept constant at 3.7 × 10<sup>-4</sup> M. In particular, the ratio of the solvent mixture was maintained at 2:1 (solvent/anti-solvent). The nanoparticles were prepared by the rapid addition of 100 μL of 3.7 × 10<sup>-4</sup> M concentration of TTBT

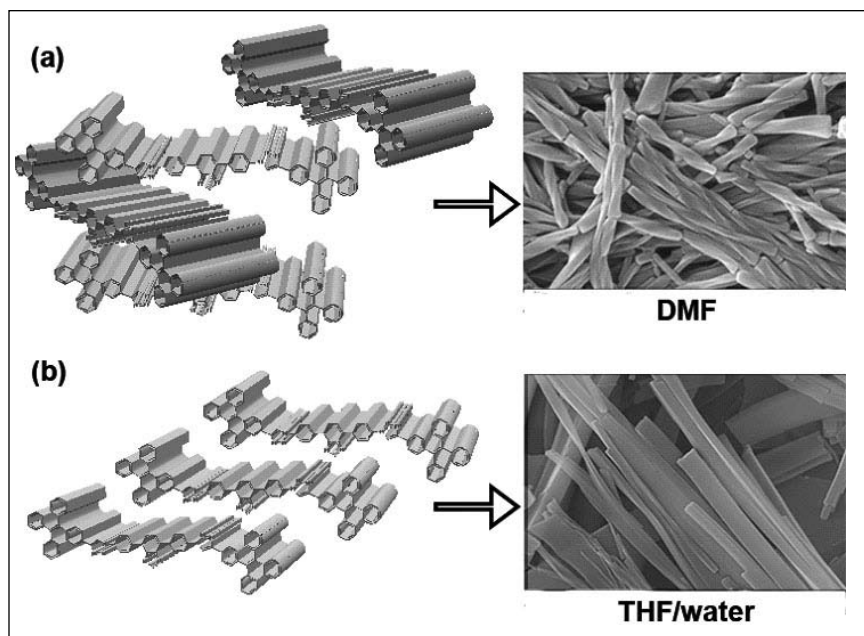


Figure 6 The self-assembly of TTBT due to the specific solvent-solute interactions in (a) DMF and (b) THF/water.

(in THF) into 2 mL of water under ultrasonication. The morphology of the self-assembled nano-structures was characterized by the field-emission scanning electron microscopy (FESEM).

## Results and discussion

TTBT exhibits almost similar absorption characteristics in DMF, DCM, EtOAc, THF and DMSO (Fig. 1a). The peak at 307 nm suggests the  $\pi$ - $\pi^*$  transition of TTBT. Whereas, the peak at 386 nm may correspond to the extended  $\pi$ -electron conjugation between the donor tetraphenylethene (TPE) and the acceptor benzothiadiazole (Bz). The change in the polarity of the solvent does not change the absorption characteristics. Although, TTBT emits in the solid state due to the presence of TPE but also fluoresce in the solution state because of the facile electronic communication between the donor (TPE) and the acceptor (Bz). It is interesting to note that, TPE shows very weak emission in solution as the excited state energy is dissipated by the intramolecular rotation (IMR) of C-Ph bonds. The restriction of IMR in the solid state due to crystal packing forces causes strong emission.<sup>22</sup> On the contrary, TTBT exhibits strong emission in solution, nanoparticles and the solid state. There is no significant shift observed in the emission of TTBT in the solvents like DMF, DMSO, EtOAc and THF (Fig. 1b). But, the photoluminescence intensity decreases in highly polar solvent DMSO when compared to the emission intensity in THF (Fig. 2).

The decrease in the fluorescence intensity of TTBT can be attributed to the hindrance to the intramolecular charge

transfer (ICT) from the donor (TPE) to the acceptor (Bz) in the polar solvent (DMSO). We expect the different emission intensity is due to the propensity of the ICT states in different solvent polarity. However, the specific quenching of fluorescence in DMSO requires further attention. The initial spectroscopic results motivated us to study the morphology of the TTBT in different solvents varying the polarity of the solution. The rapid addition of THF solution to water led to the formation of spherical nanoaggregates (Fig. 3a). In 1:2 THF/water mixture, we observed that TTBT self-assembled to rod-like structures with 0.6  $\mu\text{m}$  thickness and few microns long (Fig. 3b). The formation of self-assembled rod-like structures in THF is mostly because of the dipole-dipole interactions along the axial position, that

enhances the growth of the assemblies in one direction and decreasing its diameter.<sup>24</sup> The similar observation was noticed in the case of assemblies obtained from THF/MeOH mixture (Fig. 3c). The formation of nanorods in the THF/water or MeOH/water mixture can be attributed to the enhancement of uniform intermolecular interaction between the TTBT molecules. The  $\pi$ - $\pi$  stacking between the TTBT molecules is likely to enhance with the increment of the aqueous environment resulting in the formation of nanorods.<sup>25</sup>

In pure DMSO as a solvent, TTBT self-assembled in the form of twisted rods (Fig. 4a), unlike the assemblies formed in the case of THF/Water mixture (Fig. 3).<sup>26</sup> It is likely, that the assemblies formed in the THF/water mixture are based on the dipole-dipole interactions between the TTBT molecules which ultimately diminished in the case of DMSO, stabilizing the assemblies in a twisted manner with a possible reduction of the charge transfer. In DMSO we expect, a very weak  $\pi$ - $\pi$  interactions between the TTBT molecules losing the stacks and resulting in the formation of twisted morphologies. This can only be possible if the polar solvent molecules interact with the acceptor unit (benzothiadiazole) of the TTBT resulting in the formation of twisted structures.<sup>27</sup>

The self-assembly of TTBT in DMF completely stabilizes in a helical fashion with a typical diameter of 60-70 nm and 0.6  $\mu\text{m}$  in length (Fig. 4c). The strong polarization effect in DMF assembles the linear donor-acceptor based system into a uniform helical nanostructure without much altering its fluorescence property (Fig. 1 and Fig. 5). The

strong polarization effect in DMF reduces the  $\pi$ - $\pi$  stacking and stabilizes the aggregates in the helical fashion. The self-assembly process of the TTBT in THF/water mixture is mostly operated by the  $\pi$ - $\pi$  stacking mechanism (Fig. 6a).<sup>25</sup> Whereas, the formation of helical nanoassemblies of TTBT in the polar solvents, e.g., DMF and DMSO, are likely to be operated by the dipole-dipole interactions, stabilizing the aggregates in a twisted manner (Fig. 6b).<sup>24,27</sup>

## Conclusion

Herein, we developed a novel linear molecule based on tetraphenylethylene, triazole and benzothiadiazole, TTBT exhibiting strong fluorescence in solution, nanoparticles and solid-state. The strong fluorescence in the solid as well as in the solution state is due to the charge transfer phenomenon between tetraphenylethylene and benzothiadiazole. Interestingly, TTBT is capable of self-assembling into various 1D nanorods in aqueous solvent mixtures whereas, in polar solvents it self-assembled to twisted nanostructures, i.e., forming 1D-helices. This work shows a new fluorophore with a donor-acceptor pair linked with the  $\pi$ -conjugated spacer can efficiently self-assemble to helices showing green fluorescence in the solid state. The strong green emission in different physical states and the self-assembling characteristics make the system promising for further exploration in optoelectronic devices and as a cellular imaging agent.

## Acknowledgement:

Financial support from BRNS, DAE (no. 37(2)/14/06/2016-BRNS/ 37020) and infrastructural support from IISER Bhopal are gratefully acknowledged. WH thank UGC for fellowship.

## References

1. F. J. M. Hoeben, P. Jonkheijm, E. W. Meijer, A. P. H. J. Schenning, *Chem. Rev.*, **2005**, *105*, 1491-1546.
2. A. R. Hirst, B. Escuder, J. F. Miravet, D. K. Smith, *Angew. Chem. Int. Ed.*, **2008**, *47*, 8002-8018.
3. T. Shimizu, M. Masuda, H. Minamikawa, *Chem. Rev.*, **2005**, *105*, 1401-1444.
4. D. Lensen, D. M. Vriezema, J. C. M. van Hest, *Macromol. Biosci.*, **2008**, *8*, 991-1005.
5. M. Antonietti, S. Förster, *Adv. Mater.*, **2003**, *15*, 1323-1333.
6. J. Barauskas, M. Johnsson, F. Tiberg, *Nano Lett.*, **2005**, *5*, 1615-1619.
7. H. Wei, X. Zhang, C. Cheng, S.X. Cheng, R.X. Zhuo, *Biomaterials* **2007**, *28*, 99-107.
8. (a) S. C. Zimmerman, F. Zeng, D. E. C. Reichert, S. V. Kolotuchin, *Science* **1996**, *271*, 1095;(b) Q. Ouyang, P. D. Kaplan, S. Liu, A. Libchaber, *Science* **1997**, *278*, 446.
9. (a) S. Qu, L. Wang, X. Liu, M. Li, *Chem. Eur. J.*, **2011**, *17*, 3512-3518;(b) R. Iwaura, K. Yoshida, M. Masuda, K. Yase, T. Shimizu, *Chem. Mater.*, **2002**, *14*, 3047-3053.
10. Y. Che, A. Datar, X. Yang, T. Naddo, J. Zhao, L. Zang, *J. Am. Chem. Soc.*, **2007**, *129*, 6354-6355.
11. Y. Yamamoto, T. Fukushima, Y. Suna, N. Ishii, A. Saeki, S. Seki, S. Tagawa, M. Taniguchi, T. Kawai, T. Aida, *Science* **2006**, *314*, 1761.
12. E. Lee, J. K. Kim, M. Lee, *Angew. Chem. Int. Ed.*, **2008**, *47*, 6375-6378.
13. A. Patra, N. Venkatram, D. N. Rao, T. P. Radhakrishnan, *J. Phys. Chem. C*, **2008**, *112*, 16269-16274.
14. L. C. Palmer, S. I. Stupp, *Acc. Chem. Res.*, **2008**, *41*, 1674-1684.
15. A. Ajayaghosh, V. K. Praveen, *Acc. Chem. Res.*, **2007**, *40*, 644-656.
16. I. Böhm, K. Isenbügel, H. Ritter, R. Branscheid, U. Kolb, *Angew. Chem. Int. Ed.*, **2011**, *50*, 7407-7409.
17. X. Zhang, X. Zhang, K. Zou, C. S. Lee, S. T. Lee, *J. Am. Chem. Soc.*, **2007**, *129*, 3527-3532.
18. M. Fathalla, A. Neuberger, S. C. Li, R. Schmehl, U. Diebold, J. Jayawickramarajah, *J. Am. Chem. Soc.*, **2010**, *132*, 9966-9967.
19. A. Patra, N. Hebalkar, B. Sreedhar, M. Sarkar, A. Samanta, T. P. Radhakrishnan, *Small* **2006**, *2*, 650-659.
20. L. J. Chen, Y. Y. Ren, N. W. Wu, B. Sun, J. Q. Ma, L. Zhang, H. Tan, M. Liu, X. Li, H.B. Yang, *J. Am. Chem. Soc.*, **2015**, *137*, 11725-11735.
21. A. Patra, C. G. Chandaluri, T. P. Radhakrishnan, *Nanoscale* **2012**, *4*, 343-359.
22. Y. Hong, J. W. Y. Lam, B. Z. Tang, *Chem. Soc. Rev.*, **2011**, *40*, 5361-5388.
23. J. Wang, J. Mei, E. Zhao, Z. Song, A. Qin, J. Z. Sun, B. Z. Tang, *Macromolecules* **2012**, *45*, 7692-7703.
24. L. Li, R. Wu, S. Guang, X. Su, H. Xu, *Phys. Chem. Chem. Phys.*, **2013**, *15*, 20753-20763.
25. M. R. Islam, P. R. Sundararajan, *Phys. Chem. Chem. Phys.*, **2013**, *15*, 21058-21069.
26. W. Z. Yuan, F. Mahtab, Y. Gong, Z. Q. Yu, P. Lu, Y. Tang, J. W. Y. Lam, C. Zhu, B. Z. Tang, *J. Mater. Chem.*, **2012**, *22*, 10472-10479.
27. Y. Eom, Y. Park, Y. M. Jung, B. C. Kim, *Polymer* **2017**, *108*, 193-205.



**MD. Waseem Hussain** spent his childhood in Hyderabad, Andhra Pradesh, India. He received his B.Sc. and M.Sc. degree from Osmania University. At present, he is pursuing Ph.D. under the supervision of Dr. Abhijit Patra in the Department of Chemistry, at Indian Institute of Science Education and Research, Bhopal. His research interest is towards the fabrication of porous polymers for CO<sub>2</sub> capture and conversion. In addition, he is also interested in the design and fabrication of new fluorescent molecules and materials.



**Abhijit Patra** was born in West Bengal, India and received his early education from there. He obtained his M.Sc. degree in Chemistry from the University of Burdwan, Bardhaman in 2003 and working under the supervision of Prof. T. P. Radhakrishnan, his Ph.D. degree from the University of Hyderabad in 2009. Following a post-doctoral stint with Prof. Keitaro Nakatani in PPSM, ENS Cachan, France, he moved to the University of Wuppertal, Germany as an Alexander von Humboldt researcher in the group of Prof. Ullrich Scherf. Currently, he has been working as an Assistant Professor in the Department of Chemistry in IISER Bhopal. His research interests span various domains and facets of porous polymers and optical materials based on molecular and polymeric assemblies and nanomaterials.

## Influence of particle size of albumin nanoparticles on its drug loading and cellular uptake.

Beena G. Singh<sup>1\*</sup>, Ram P. Das<sup>1</sup>, Amit Kunwar<sup>1</sup>

<sup>1</sup>Radiation & Photochemistry Division, Bhabha Atomic Research Centre, Trombay, Mumbai - 400085  
E-mail: beenam@barc.gov.in

### Abstract

To elucidate the effect of particle size of albumin nanoparticles on cellular uptake of hydrophobic drug, herein we report the preparation of bovine serum albumin (BSA) nanoparticles of different sizes and comparable surface potential and their abilities to release dimethylcurcumin (DMC), a model for hydrophobic drug in A549 tumor cells. The nanoparticles were prepared by thermal denaturation and characterized by dynamic light scattering (DLS) and zeta ( $\zeta$ ) -potential measurements. The preparation conditions were optimized to obtain nanoparticles of sizes  $28.0 \pm 0.3$  nm (BSAnp1) and  $52.0 \pm 1.0$  nm (BSAnp2) with corresponding  $\zeta$ -potential value of  $\sim -7.0$  and  $-6.0$  mV respectively. Loading of DMC was higher in BSAnp2 as compared to BSAnp1 and BSA native, which is attributed to the presence of higher hydrophobic sites. Uptake studies indicated that intracellular delivery of DMC increased with an increase in particle size and the toxicity of DMC loaded nanoparticles were found to be in correlation with their cellular uptake. Thus, BSAnp2 can be used as an effective delivery system for hydrophobic drugs like DMC and highlights the importance of particle size in dictating the release of drug.

### Introduction:

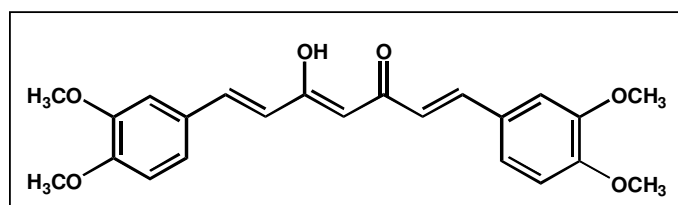
The growth of nanotechnology has opened several new possibilities in drug delivery as they confer advantageous properties like higher surface to mass ratio that enhances their ability to bind, adsorb and carry drugs.<sup>[1, 3]</sup> Along with these physico-chemical parameters, new methods to prepare a given size with desired surface properties bestow these nanocarriers to release drugs at a therapeutically optimal rate and dosage regimen.<sup>[1, 2]</sup> With the advent of these nanocarriers, many diseases are now treated with higher efficacy. Among these one of the major areas where their development is utilized to the maximum possible extent is for the treatment of cancer. The action of conventional chemotherapeutics has been marred with many drawbacks like systemic toxicity due to a lack of specificity, selectivity, higher toxicity to normal cells and low bioavailability due to first pass metabolism.<sup>[2, 3]</sup> In this context, nanoparticle-based drug delivery systems play a vital role.<sup>[5, 8]</sup> Nanocarrier used for drug delivery systems are an inert matrix which encapsulates drug molecules by binding through non-covalent or covalent attachment. This provides high stability to the drug, prevents its metabolic degradation, increases the circulation time of the drug and minimizes their toxicity. In this regard, several drug delivery systems have been studied, which employ a number of biocompatible nanocarriers like oil in water emulsions<sup>[3, 4]</sup>, nanocapsules, liposomes<sup>[5, 6]</sup> and protein nanoparticles<sup>[7-9]</sup>. Among these systems, protein nanoparticles have gained considerable interest

in recent years due to low toxicity, non-immunogenic and biodegradable nature.<sup>[10-11]</sup>

Bovine Serum Albumin (BSA) is a well-known model system that mimics human serum albumin, a major soluble protein of the circulatory system and its concentration in the blood is reported to be  $\sim 50$  mg/ml. It is involved in the transport of nutrients to cells and maintenance of osmotic pressure.<sup>[12]</sup> The high solubility of albumin (upto 40% w/v) at pH 7.4 makes it an attractive macromolecular carrier capable of accommodating a wide variety of drugs. Albumin nanoparticles are biodegradable, can be prepared in well defined sizes under mild condition, and possess functional groups (thiol, amino, and carboxylic groups) that can be used for surface modifications. Importance of albumin-based nanoparticles as drug delivery agents for anti-cancer drugs are gaining importance due to the fact that they accumulate selectively in tumor sites, via complementary pathways such as enhanced permeation retention (EPR) effect, and receptor (gp60 and SPARC)-mediated transcytosis at tumor site.<sup>[15-17]</sup> The most successful albumin nano therapeutics are Abraxane (albumin-bound formulation of paclitaxel) and Aldoxorubicin (albumin bound to doxorubicin).<sup>[7]</sup>

After the success of albumin based nanocarriers, most of the studies are focussed on modulating the surface properties of the carrier to influence their pharmacokinetic properties. However, along with surface properties, the particle size of the nanocarrier may also influence the cellular uptake. Indeed, there are few reports in literature

on this aspect. However, the optimum particle size to achieve maximum cellular uptake remains unexplored. DMC (structure given in Scheme 1), a synthetic analogue of curcumin is used as a model hydrophobic drug. DMC has been found to be about three fold more metabolically stable and is more effective anti-inflammatory and anti-tumour agent than curcumin. However its low bioavailability due to poor absorption is a major drawback. The present study was thus carried out to address the effect of particle size on binding and subsequent release of drug using DMC as a model hydrophobic compound. For this the binding of DMC with BSA<sub>np</sub> has been studied by employing absorption technique and the uptake of these complexes was evaluated in a human lung cancer cell line (A549).



Scheme 1: Structure of Dimethylcurcumin (DMC)

### Characterization of BSA nanoparticles

BSA is a water soluble protein known to undergo thermal denaturation and susceptible to agglomeration to form nanoparticles. Thermal induced aggregation of BSA depends on different factors such as temperature, pH, protein and salt concentration. Thus, the reaction condition was optimized to obtain nanoparticles of different sizes. In the present work, size selective particles were prepared by temperature controlled denaturation of 1% w/v BSA solution at 65 °C and 69 °C. The formation of BSA nanoparticles was monitored by DLS technique (Fig. 1). The particle size was estimated by fitting the intensity correlation function using the cumulants method to obtain average relaxation time of the correlation function, which is related to the diffusion coefficient of the particles. The average hydrodynamic diameter of the particle is calculated from the diffusion coefficient using Stokes-Einstein equation. The average hydrodynamic size of BSA native solution is found to be 8.0 nm (P. I. 0.097), consistent with the size expected from BSA monomers. Upon heat treatment at 65 °C and 69 °C, the average diameter increased to 28.0 ± 0.3 nm (BSA<sub>np1</sub>, P.I. 0.147) and 52.0 ± 1.0 nm (BSA<sub>np2</sub>, P.I. 0.175), respectively, indicating aggregation of BSA. The temperature range of 65-70°C is crucial to control the particle size of BSA nanoparticles and heating below this temperature did not produce any aggregates, while heating above 70 °C leads to precipitation of large aggregates from the suspension. The formation of nearly globular aggregates after thermal

denaturation is supported by TEM, where it was observed that BSA nanoparticles were nearly spherical in shape with approximately same size as observed by DLS. Further, BSA nanoparticle was characterized by zeta ( $\zeta$ ) potential measurements. The  $\zeta$ -potential of BSA native form was estimated to be  $-8.95 \pm 0.82$  mV which decreased to  $-7.35 \pm 0.57$  and  $-6.78 \pm 0.48$  mV in case of BSA<sub>np1</sub> and BSA<sub>np2</sub>, respectively. The BSA nanoparticles prepared herein are free from external cross-linking agent and solvents making it a green route for nanoparticles synthesis.

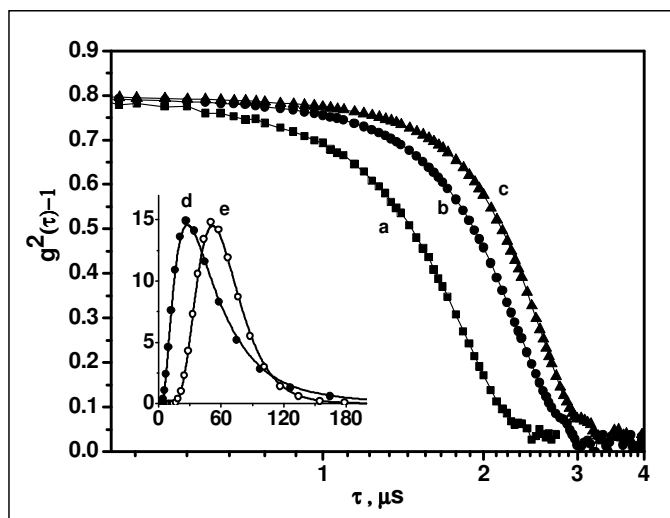


Figure 1: Plot of variation of normalized intensity correlation function as a function of correlation time obtained for 1% BSA native (a), BSA<sub>np1</sub> (b) and BSA<sub>np2</sub> (c). Inset shows the size distribution of BSA<sub>np1</sub> (d) and BSA<sub>np2</sub> (e).

### Loading of DMC into BSA nanoparticles:

The effect of particle size on the loading of DMC in BSA nanoparticles were studied and compared with the native protein. The encapsulation efficiency of 1% aqueous BSA solution mixed with 130  $\mu$ g of DMC was estimated to be  $39 \pm 3.1$  %,  $57.0 \pm 4.7$  % and  $85.7 \pm 5.3$  % for BSA native, BSA<sub>np1</sub> and BSA<sub>np2</sub>, respectively. Thus, the encapsulation efficiency of DMC in BSA strongly depends on the particle size and nature of the protein. The higher loading in BSA<sub>np2</sub> as compared to BSA<sub>np1</sub> and BSA native may probably be attributed to higher hydrophobic sites in the bigger nanoparticles.

The existence of hydrophobic pocket was further confirmed by monitoring the binding of BSA nanoparticles and native form with fluorescence dye like 8-anilino-1-naphthalenesulfonic acid (ANS), which are used as a reporter to probe hydrophobicity of a system. ANS is practically non-fluorescent in water but its fluorescence intensity increases upon binding to hydrophobic sites of

protein. Thus, the aqueous solution of ANS upon excitation at 345 nm, showed the emission at 515 nm with low intensity. However, in presence BSA native, the emission maximum showed blue shift at 455 nm with increase in fluorescence intensity. Under identical experimental condition, the fluorescence maxima of ANS remained similar in BSA nanoparticles, but its intensity increased by a factor of 4 to 4.5 times as compared to aqueous solution. The increase in the fluorescence intensity was in the order BSA<sub>np2</sub>>BSA<sub>np1</sub>> BSA native form. These results suggested that increase in average size of BSA nanoparticles makes it more hydrophobic in nature and leads to enhanced binding of hydrophobic molecules like DMC.

### Drug release and cytotoxicity evaluation

The efficacy of the drug carrier depends on its sustainability to release the drug payload and therefore it is imperative to understand the release kinetics of the drug from BSA nanoparticles and compare it with BSA native form. The release profile of DMC from native and BSA nanoparticles was investigated under reservoir-sink condition (reservoir: pH 7 containing 0.1 % Tween 80, sink: pH 7.4) at 37 °C. The release of DMC from the protein showed time dependent release profile. As observed in fig. 2, the release profile is significantly altered upon formation of nanoparticles. At short times (less than 50 hrs) the native form showed fast release as compared to BSA nanoparticles. However, at long time (> 50 hrs) the behavior is different for BSA<sub>np2</sub>, as compared to native BSA and BSA<sub>np1</sub>. For example, at 80 hrs, it was observed that BSA<sub>np2</sub>, BSA<sub>np1</sub> and native released 70%, 50% and 45% of DMC, respectively. The results indicated that BSA nanoparticles showed sustained release of the drug, as compared to that from BSA native.

The slow release of DMC from BSA nanoparticles is consistent with previous reports on the release of other hydrophobic drug from macromolecular drug delivery systems and can be ascribed to the higher hydrophobic sites in BSA<sub>np1</sub> and BSA<sub>np2</sub> as compared to native form. The sustained release of DMC by BSA nanoparticles was reflected on its uptake and toxicity profile in A549 cells. In brief, uptake of free DMC (dissolved in DMSO) marginally increased in a time (2hr to 10 hr) dependent manner. On the other hand, DMC bound to BSA<sub>np2</sub> although showed higher uptake compared to free DMC at all the time points, the fold difference increased with the increasing time of incubation (fig. 3A). In line with these observations, DMC bound to BSA<sub>np2</sub> nanoparticles showed significantly higher toxicity at 72 hr compared to 48 hr. Whereas DMC in DMSO or native BSA showed no change in cytotoxicity with increasing time (fig. 3B). The higher toxicity by BSA<sub>np2</sub> at delayed time is consistent with the previous observation of sustained release and higher delivery by this formulation with time. The BSA (1%) in native as well as nanoparticle forms without DMC did not cause any cytotoxicity. The difference in the delivery of DMC by BSA through different formulations is

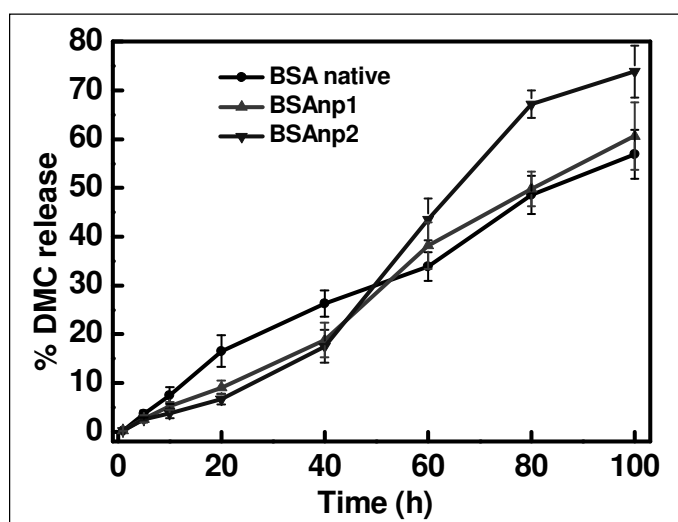


Figure 2: Amount of DMC release in terms of percentage at different time from different form of BSA (● BSA native, ▲ BSA<sub>np1</sub> and ▼ BSA<sub>np2</sub>).

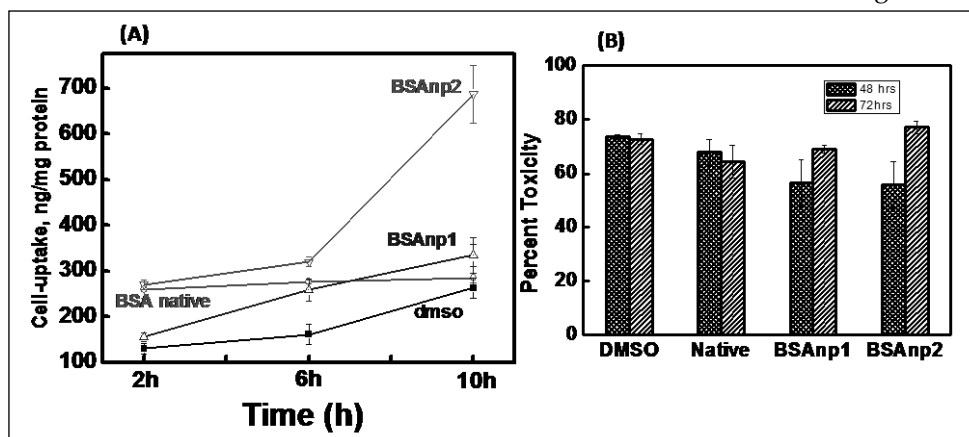


Figure 3: Panel (A) shows cellular uptake of 12.5 μM DMC by A549 cell lines using different carrier (a) 0.15 % DMSO, (b) BSA native, (c) BSA<sub>np1</sub> and (d) BSA<sub>np2</sub> at different time points. Panel (B) shows the comparison of toxicity in A549 cell line following treatment with 10 μM DMC loaded in different carriers (DMSO, BSA native, BSA<sub>np1</sub> and BSA<sub>np2</sub>) at 48 hrs and 72 hrs.

due to their different mechanism of cellular interaction. Albumin proteins release drug molecules to the target cells via fluid phase pinocytosis, while nanoparticles are reported to release drug molecules via endocytosis.<sup>[18]</sup> It is reported that uptake of albumin nanoparticle decorated with poly(methylmethacrylate) and poly( $\epsilon$ -caprolactone) polymer takes place predominantly via caveolae-mediated endocytosis.<sup>[19]</sup> With similar analogy, it can be expected that the uptake of DMC via albumin nanoparticles used in present study takes place via endocytosis.

Further the significance of present study is that the BSA nanoparticles have been prepared by thermal denaturation. It is worth to mention that BSA nanoparticles prepared by this method are non-toxic unlike to other protein fibril. Otzen et al have suggested that BSA on thermal denaturation retains significant amount of  $\alpha$ -helical structure and lack a protease-resistant core, which is responsible for their non-toxic nature.<sup>[20]</sup> Recent reports indicate that non-continuous endothelia with vascular fenestrations in the liver (measuring 50–100 nm) along with splenic filtration leads to nonspecific accumulation of larger particles >200 nm in these organs, thus decreasing their circulation time. Based on this, it is suggested that the optimum nanoparticles size to have longer circulation is ~ 100 nm. In the present study, BSAnp2 loaded with DMC has an average particle size of ~60 nm and shows cyto-toxicity upto 90% at 72 hrs of treatment. Thus, BSAnp2 appears to be the appropriate delivery system for controlled release of the drug over a period of time and induce toxicity in tumor cells.

### Conclusions:

Two different size of BSA nanoparticles are prepared by thermal denaturation and their abilities to carry and deliver DMC, a curcumin analogue have been estimated. Throughout the study results are compared with native BSA form. Finally, the ability of the nanoformulation for efficient loading of DMC and its release in A549 cells were also investigated. Under identical concentrations of DMC, the BSAnp2 facilitates higher uptake and cytotoxicity than BSAnp1, native form or the DMSO-aqueous form.

### Acknowledgement:

The authors acknowledge the support and encouragement from Drs. K. I. Priyadarsini (Head, Chemistry Division, BARC) and P. D. Naik (Assoc.

Director, Chemistry Group, BARC). The authors also acknowledge Dr. P. A. Hassan for his help in dynamic light scattering experiments. They also acknowledge M. V. Ramani, G. V. Subbaraju, from Natsol Laboratories Pvt. Ltd for gifting dimethyl curcumin.

### References:

1. T. Sun, Y. S. Zhang, B. Pang, D. C. Hyun, M. Yang, Y. Xia, *Angew. Chem. Int. Ed.* **2014**, 53 12320 – 12364.
2. R. P. Das, B. G. Singh, A. Kunwar, M. V. Ramani, G. V. Subbaraju, P. A. Hassan, K. I. Priyadarsini, *Colloids surf. B Biointerfaces*, **2017**, 158, 682-688.
3. K. Krukiewicz, J. K. Zak, *Materials Science and Engineering C*, **2016**, 62, 927-942.
4. J. I. Harea, T. Lammers, M. B. Ashforde, S. Purie, G. Stormc, S. T. Barrya, *Adv. Drug Deliv. Rev.*, **2017**, 108, 25-38.
5. F. Muzaffar, U. K. Singh, L. Chauhan, *Int. J. Pharm. Pharm. Sci.*, **2013**, 5, 39-53.
6. J. K. Saini, U. Nautiyal, M. S. Kumar, D. Singh, F. Anwar, *Int. J. Pharm. Med. Res.*, **2014**, 2, 15-20.
7. T. M. Allen, P. R. Cullis, *Adv. Drug Deliv. Rev.*, **2013**, 65, 36-48.
8. Y. Malam, M. Loizidou, A. M. Seifalian, *Trends Pharmacol. Sci.*, **2009**, 30, 592-599.
9. E. Miele, G. P. Spinelli, E. Miele, F. Tomao, S. Tomao, *Int. J. Nanomedicine*, **2009**, 4, 99-105.
10. M. Jahanshahi, Z. Babaei, *Afr. J. Biotechnol.*, **2008**, 7, 4926-4934.
11. X. He, N. Xiang, J. Zhang, J. Zhou, Y. Fu, T. Gong, Z. Zhang, *Int. J. Pharm.*, **2015**, 487, 250-259.
12. A. O. Elzoghby, W. M. Samy, N. A. Elgindy, *J. Control. Release*, **2012**, 157, 168-182.
13. K. S. Soppimath, T. M. Aminabhavi, A. R. Kulkarni, W. E. Rudzinski, *J. Control Release*, **2001**, 70, 1-20.
14. J. J. Marty, R. C. Oppenheim, P. Speiser, *Pharm. Acta Helv.*, **1978**, 53, 17-23.
15. J. Wu, J. M. Prausnitz, *Fluid Phase Equilib.*, **1999**, 155, 139-154
16. H. Niknejad, R. Mahmoudzadeh, *Iran J. Pharm. Res.*, **2015**, 14, 385-394.
17. A. M. Merlot, D. S. Kalinowski, D. R. Richardson, *Front Physiol.*, **2014**, 5, 299-305.
18. N. Oh, J. H. Park, *Int. J. Nanomedicine*, **2014**, 9, 51 - 63.
19. Y. Jiang, M. Stenzel, *Macromol. Biosci.* **2016**, 16, 791-802.
20. N. K. Holm, S. K. Jespersen, L. V. Thomassen, T. Y. Wolff, P. Sehgal, L. A. Thomsen, G. Christiansen, C. B. Andersen, A. D. Knudsen, D. E. Otzen, *Biochim. Biophys. Acta*, **2007**, 1774, 1128 - 1138.

	<p><b>Dr. Beena G. Singh</b> has received her Ph.D. degree in Chemistry from University of Mumbai. She had joined Bhabha Atomic Research Centre, India as a K. S. Krishnan Research Associate and later promoted as a scientist in Radiation &amp; Photochemistry Division in the same institute. Her area of interest is Radiation Chemistry and application of biophysical technique in understanding the interaction of drugs with macromolecules. She is the recipient of Scientific &amp; Technical Excellence Award-2015, Department of Atomic Energy.</p>
	<p><b>Mr. Ram Pada Das</b> has obtained his M.Sc. degree in Chemistry from I.I.T. Kanpur. He has joined Bhabha Atomic Research Centre, India as Scientific Officer/C in Radiation &amp; Photochemistry Division after successfully completing one year Orientation Course in Engineering and Science from BARC Training School, Mumbai. His current research interest includes basic understanding of soft material based nano drug delivery system and their application in cancer chemotherapeutics</p>
	<p><b>Dr. Amit Kunwar</b> joined Radiation &amp; Photochemistry Division, BARC in 2005 after graduating from BARC Training School (48<sup>th</sup> Batch, Bioscience discipline). He completed his Ph.D. from the Homi Bhabha National Institute in 2010, and following this carried out his postdoctoral research at Meakins Christie Laboratories, McGill University, Montreal, Canada, 2012-2014. He is the recipient of "Lester Pecker Young Investigator Award-2010" from the Oxygen Club of California, USA, "Young Scientist Award -2010" from DAE, "Richard and Edith Strauss Postdoctoral Fellowship in Respiratory Medicine" from the faculty of medicine, McGill University.</p>

# Effect of Zinc Oxide Nanoparticles on DC Electrical Conductivity of Inorganic-Organic Conducting Nanocomposites

Shahid Pervez Ansari and Faiz Mohammad\*

Department of Applied Chemistry, Faculty of Engineering and Technology, Aligarh Muslim University, Aligarh, India-202002  
E-mail: faizmohammad54@rediffmail.com

## Abstract

Inorganic-organic conducting nanocomposites of polyaniline, zinc oxide nanoparticles and polyvinylchloride were prepared by solution casting method at ambient condition using N-methyl-2-pyrrolidone as solvent. These nanocomposites were studied for role of zinc oxide nanoparticles on the DC electrical conductivity and its stability in terms of DC electrical conductivity retention using four-in-line probe technique under two different conditions, *i.e.* isothermal aging and cyclic aging. The electrical conductivity nanocomposites was found to be dependent mainly on polyaniline, however, presence of zinc oxide nanoparticles have played an important role in controlling it due to possible interaction of polyaniline and zinc oxide nanoparticles. All the nanocomposite samples followed Arrhenius equation for the temperature dependence of electrical conductivity and support the semi-conducting nature of the doped nanocomposites. The studied samples showed good electrical conductivity stability upto the temperature of 90°C. These nanocomposites may find promising application sensing and electroanalytical techniques.

## Introduction

Recent past has witnessed an intense research in the area of nanocomposites. Nanostructures and nanocomposites of conducting polymers have emerged as new field dedicated to creation of smart materials for future technologies<sup>1,2</sup>. Nanocomposites containing inorganic nanoparticles in intrinsically conducting polymer matrix are believed to be promising materials of tomorrow. It is because of the interaction of inorganic nanoparticles with delocalized  $\pi$ -electrons in conjugated polymers and endows them special properties<sup>3</sup>. Studies on polymer nanocomposites and especially conducting polymer nanocomposites including studies involved to find new advanced material with improved mechanical, electrical, optical and catalytic properties of nanocomposites or to improve conduction mechanism in electronic devices<sup>3</sup>. Generally, there are three major approaches to prepare organic-inorganic nanocomposite which include (i) direct mixing in a common solvent, (ii) in situ polymerization of monomer units in presence of filler material and melt-mixing of inorganic particle and polymeric material in mixer<sup>4</sup>.

Among intrinsically conducting polymers, polyaniline (PANI), owes a reputed position and it is widely studied. Easy preparation, excellent stability, easy acid/base doping/dedoping, reversible redox behavior and controllable electrical conductivity between insulating to semiconducting and conducting materials are some special properties of PANI<sup>5-7</sup>. There are several reports on

the synthesis of the nanocomposites of PANI with TiO<sub>2</sub>, CdS, Na<sup>+</sup>- montmorillonite, Pd or Au nanoparticles have been described<sup>1,3,8</sup>.

In present work, we have used zinc oxide (ZnO) nanoparticles as inorganic filler, polyaniline (PANI) as main matrix and polyvinylchloride (PVC) as supporting matrix. It is because of the facts that among inorganic nanoparticles, ZnO has received great attention because of its unique catalytic, electrical, electronic, optical properties, low production cost and extensive applications in diverse areas<sup>9</sup>. On the other hand, PVC is a widely used polymer due to its stability against acid and bases, lower cost of production<sup>10, 11</sup>, recent reports have proposed its use in membrane material in gas separation and various polymer electrolyte systems<sup>12</sup> and PANI:PVC composite in ammonia sensors<sup>13</sup>. The electrical conductivity and stability in terms of electrical conductivity retention of the prepared conducting nanocomposites have been studied here in this communication.

## Materials and methods

### Materials:

The materials used during the experiments were acetone (merck, India), ammonia (Qualigen, India), aniline (merck, India) double distilled prior to experiment, HCl (Rankem, India), N-methyl-2-pyrrolidone (NMP) (Qualigen, India), polyvinyl chloride (PVC) (GSK chemicals, Mumbai, India), potassium persulphate (CDH, India), and zinc oxide nanoparticles (ZnO) (avg. size 50 nm) (mknano, Canada).

### Preparation of polyaniline:

Polyaniline (PANI) was prepared by oxidative polymerization of aniline in aqueous HCl (1M) solution. The oxidative polymerization of aniline in HCl (1M) was obtained using potassium persulphate ( $K_2S_2O_8$ ) as oxidant in HCl (1M)<sup>14, 15</sup>. In acidic medium, aniline is present as anilinium cation and predominate aniline molecules in equilibrium condition. Aniline undergoes oxidation to give non-conducting oligomers, however, anilinium cations on oxidation give conducting polyaniline. The optimum ratio of aniline:oxidant (2:1) was kept constant during the reaction. Desired volumes of aniline and potassium persulphate ( $K_2S_2O_8$ ) in HCl (1M) were separately cooled to 0-5°C in refrigerator; the two solutions were mixed for complete polymerization. PANI (Emeraldine Salt) so obtained, filtered and washed with double distilled water till filtrate became neutral to pH paper followed by its dedoping using 1M ammonia solution to get emeraldine base, one of the non-conducting form of PANI, which after through washing and drying at 60°C in air oven was kept in desiccators<sup>16</sup>.

### Preparation of nanocomposites:

The preparation of nanocomposite can be mainly divided into four steps, involving dispersion of ZnO

**Table 1 Preparation of nanocomposites of polyaniline (PANI), polyvinylchloride (PVC) and zinc oxide (ZnO) nanoparticles.**

Sample ID	Amount (mg) of PANI (emeraldine base) in 50 ml NMP	Amount (mg) of ZnO nanoparticles in 50 ml NMP	Amount (mg) of PVC in 50 ml NMP
PANI: PVC:Z0	950	0	50
PANI: PVC:Z1	940	10	50
PANI: PVC:Z2	930	20	50
PANI: PVC:Z3	920	30	50
PANI: PVC:Z4	910	40	50
PANI: PVC:Z5	900	50	50
NMP = N-Methyl-2-pyrrolidone			

nanoparticles, preparation of PANI(EB) and/or PVC, mixing of ZnO dispersion in PANI:PVC solution and finally drying to get film. Firstly, zinc oxide nanoparticles (ZnO) of desired quantity were dispersed in 50 ml of N-methyl-2-pyrrolidone (NMP) in a round bottom flask for 12 hrs. with continuous vigorous stirring at room temperature and in other flask, 50 mg PVC was dissolved in 50 ml NMP and to this PVC-NMP solution, required amount of polyaniline

(PANI) base form was dissolved slowly with continuous stirring. Dispersion of ZnO nanoparticles were then added to PANI:PVC solution at a rate of 1ml/min (Table 1). The films of the prepared nanocomposites solution were obtained by solvent evaporation method at 100°C in an air oven. Thus, prepared films were cut into small pieces of rectangular shape and smoothened by applying a pressure of 10 tons at 150°C using electrically operated hydraulic press machine. These films were then treated with 1M HCl for 24 hrs, washed with double distilled water repeatedly to remove traces of acid, dried at 60°C for 12 hrs. and were used for electrical studies<sup>2,5</sup>.

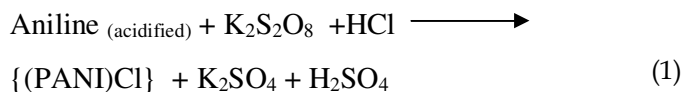
### Characterization

All the conducting nanocomposites were characterized for their DC electrical conductivity and stability in terms of DC electrical conductivity retention. DC electrical conductivity of the doped conducting nanocomposite films were measured in rising temperature mode from 40°C to 150°C using a four-in-line probe DC Electrical Conductivity Measuring Instrument (Scientific Equipments, Roorkee, India). Furthermore, selected samples of conducting nanocomposites were characterized by advance analytical techniques, FTIR using Inter-Spec 2020 (Spectro Lab, UK), scanning electron microscope (SEM) micrographs of surface of selected samples were obtained using SEM-JEOL 840 A. Transmission Electron Microscope (TEM) micrographs (Phillips CM-10) of zinc oxide nanoparticles and PANI:PVC:Z5 conducting nanocomposite and XRD of powder samples were done using X'pert Pro diffractometer. All the analyses were performed in undoped condition but electrical conductivity studies were done after HCl doping of the samples.

### Results and Discussions

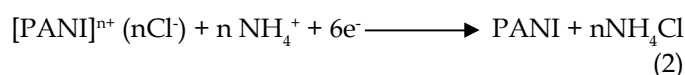
#### Preparation of PANI:

Aniline was oxidized in an acidic (HCl) aqueous medium with potassium persulphate ( $K_2S_2O_8$ ), the protonated conducting form of polyaniline {(PANI)Cl} is produced as given in the following empirical equation:



Thus, obtained polyaniline is green in color (Emeraldine salt form) is dedoped with ammonia and the color changes to blue. This color change is associated with the neutralization of positive charges on protonated polyaniline chains. The process may be treated as *n*-type doping of a *p*-type doped polymer in which the polymer passes through an insulating state. The electrical conductivity of these materials could be varied from insulator to metal through semi-conductor

range by controlling the doping level. The neutralization of charges of polymer chain depends on the rate of chemical reaction between the polymer and the dopant which in turn depend upon the reactivity of the polymer chain and the basic strength of the dopant<sup>21</sup>. The basic strength of the water is very low and hence it does not act as effective undoping agent in case of polyaniline. Neutralization reaction for the undoping of the polyaniline by ammonia may be suggested as below:



#### FTIR study:

The peak at 463 in Fig.1a can be assigned to Zn-O group<sup>18</sup>. FTIR spectrum of prepared PANI (EB) form is presented in Fig.1b. The band corresponding to out of plane bending vibration of C-H bond of *p*-disubstituted benzene rings appears at (824 cm<sup>-1</sup>)<sup>19</sup>. The bands corresponding to vibration mode of N=Q=N ring and stretching mode of C-N bond appear at (1150 cm<sup>-1</sup> and 1307 cm<sup>-1</sup>)<sup>21</sup>. Band at (1582 cm<sup>-1</sup> and 1496 cm<sup>-1</sup>)<sup>22,23</sup> are assigned to C=C stretching of quinoid and benzenoid rings respectively. The bands at 1326, 1250 and 966 cm<sup>-1</sup> in pure PVC Fig. 1c are assigned to CH<sub>2</sub> deformation, CH rocking and CH wagging respectively. The characteristic bands of PVC can be classified into three regions. The first is called the C-Cl stretching region in the range from 600-700 cm<sup>-1</sup>. The second region is called C-C stretching in the range from 900-1200 cm<sup>-1</sup>. The third region is 1250-2970 cm<sup>-1</sup> in PVC (numerous CH modes)<sup>24</sup>. In case of nanocomposite PANI:PVC:Z5 in NMP (Fig. 1d) peaks at 1298, 1678, 2879 and 2951 cm<sup>-1</sup> are characteristic peaks of NMP and characteristic peaks of PANI have blue/red shifted, it clearly defines some interactions with solvent, co-matrix polymer and zinc oxide nanoparticles<sup>25</sup>.

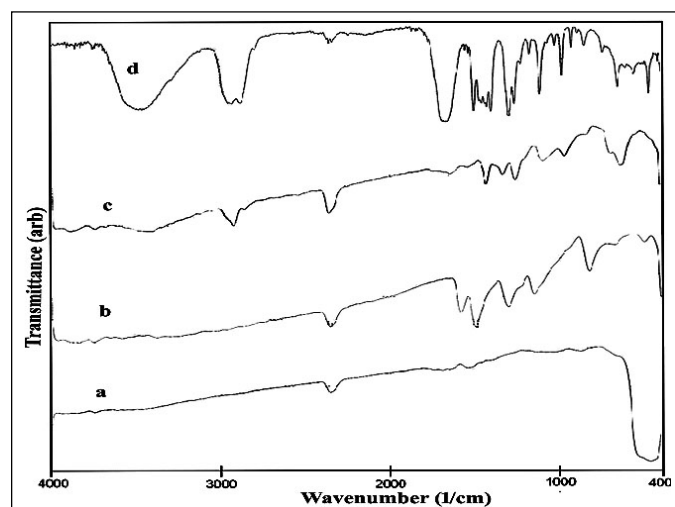


**Figure 1:** FTIR spectra of a) ZnO nanoparticles, b) PANI (EB), c) polyvinylchloride (PVC) and d) nanocomposite containing PANI:PVC: Z5.

#### Electrical conductivity study:

DC electrical conductivity of the HCl doped nanocomposite films was measured with increasing temperature (40°C -150°C) by using four-in-line probe DC Electrical Conductivity Measuring Instrument (Scientific Equipment, Roorkee, India). DC electrical conductivity ( $\sigma$ ) was calculated using following equations:

$$\rho = \rho^0 / [G_7(W/S)] \quad (3)$$

$$G_7(W/S) = (2S/W)\ln(2) \quad (4)$$

$$\rho^0 = (V/I) (2\pi S) \quad (5)$$

$$\sigma = 1/ \rho \quad (6)$$

Where  $G_7(W/S)$  is a correction divisor which is a function of thickness of the sample as well as probe spacing, I, V, W and S are current (A), voltage (V), thickness of the film (cm) and probe spacing (cm) respectively<sup>2</sup>.

The electrical conductivity of the HCl doped nanocomposite films was measured from 40°C to 150°C and electrical conductivity of all conducting nanocomposites was observed in semi-conducting region as presented in Fig. 2. All the studied samples, PANI, PANI:PVC and PANI:PVC:ZnO nanocomposites followed Arrhenius relation for temperature dependence of electrical conductivity as seen in Fig. 2 and suggest the semi-conducting nature of HCl doped nanocomposites. It may be seen from Fig. 3 that the maximum reported electrical conductivity was obtained for doped PANI, in case of nanocomposites, decrease in electrical conductivity was observed. However, in case of PANI:PVC:Z2, an increase in electrical conductivity was observed with further decrease in electrical conductivity. Eventually, it seems that PANI is mainly responsible for the electrical conductivity and in case of PANI:PVC:Z2 nanocomposite, different chemistry is involved. This can be understood with the following proposed reactions, where ZnO nanoparticles play dedoping role for the PANI. The increase in case of PANI:PVC:Z2, was due to the presence of Zn<sup>2+</sup> ions which are formed due to dedoping process. With further increase in ZnO content, dedoping behavior of ZnO predominates and electrical conductivity was decreased<sup>2,26</sup>.

#### Stability in terms of DC electrical conductivity retention

It was observed that the PANI:PVC: ZnO nanocomposites showed the enhanced conductivity on exposure to HCl, due to the involvement of charge-transfer reaction between polyaniline component and the doping agent<sup>7</sup>.

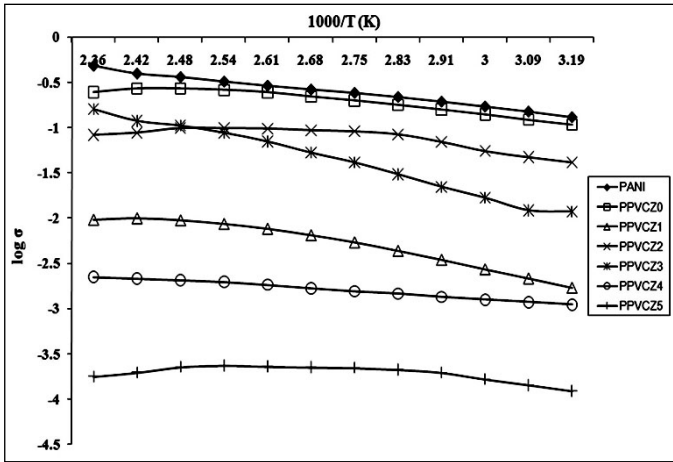


Figure 2 Arrhenius plot of HCl doped PANI and different PANI:PVC:ZnO nanocomposites.

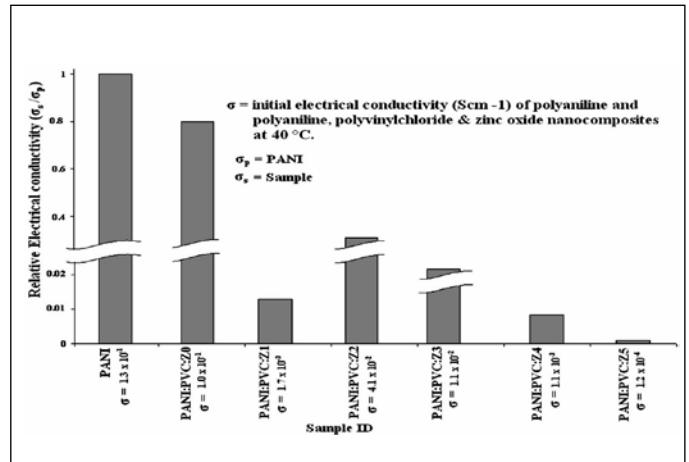


Figure 3: Schematic diagram of relative electrical conductivity of HCl doped nanocomposite films of PANI, PVC and ZnO nanoparticles with respect to HCl (1M) doped PANI film.

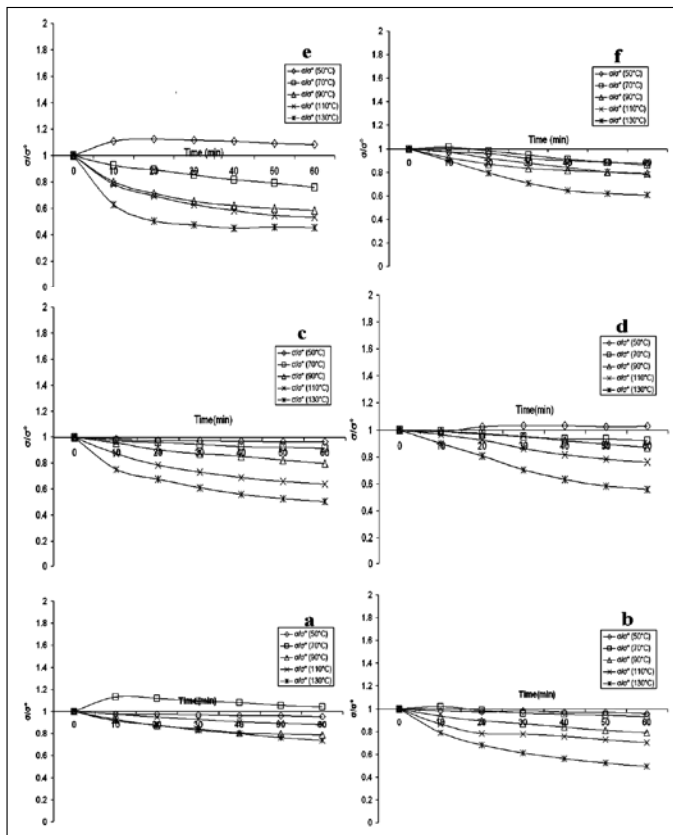
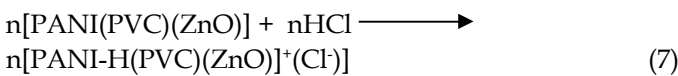


Figure 4: Electrical conductivity retention of a) PANI:PVC:Z0, b) PANI:PVC:Z1, c) PANI:PVC:Z2, d) PANI:PVC:Z3, e) PANI:PVC:Z4 and f) PANI:PVC:Z5 under isothermal ageing conditions



The conducting nanocomposite samples were also studied for the stability in terms of DC electrical conductivity by two slightly different techniques, one is

isothermal ageing condition at 50°C, 70°C, 90°C, 110°C and 130°C and the other is cyclic ageing study of DC electrical conductivity from 40°C-150°C in oxidative atmosphere. During the isothermal ageing study the temperature of the sample films were maintained at temperature of study and the DC electrical conductivity was measured at an interval of 10 min. for an hour. The DC electrical conductivity was found to be quite stable at 50°C, 70°C and 90°C and therefore, it can be said that under thermo-oxidative atmosphere, the electrical properties of the samples are sufficiently stable up-to 90°C. However, the decrease in electrical conductivity at higher temperature, can be credited to loss of dopants and crosslinking reactions within the chain of PANI at higher temperatures. This can be well supported by the data obtained from cyclic ageing studies on the various samples (Fig. 4-5). It has been found that there is loss of conductivity after first cycle in each case, which is assigned to loss of moisture in first cycle in each case. However, similar loss was observed in other four cycles, loss of conductivity was there in every next cycle but in each case only little loss of conductivity was observed. On the other hand, it was observed that with the increase in ZnO content in nanocomposites, loss in electrical conductivity decreased. Therefore, it can be suggested that with the increase in the ZnO content, the composites get thermally stable and little better than that having no inorganic filler.

### Electron microscopy study:

The Scanning Electron Microscopy (SEM) micrographs of surface of undoped polyaniline (emeraldine base) film and HCl doped PANI:PVC:Z5 nanocomposite film are given in Fig. 6. The surface of undoped polyaniline (PANI) film is irregular and wavy nature but the

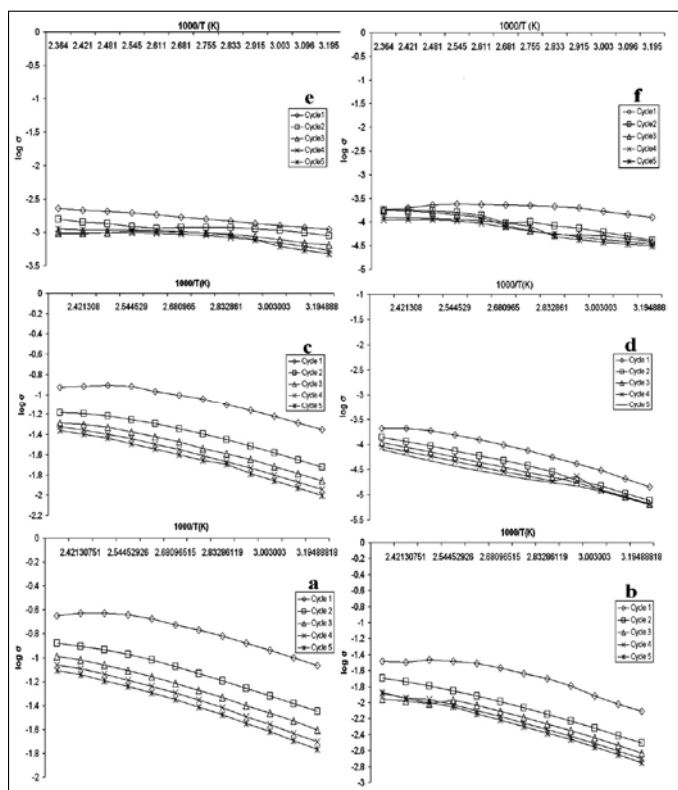


**Figure 5.** Electrical conductivity retention of a) PANI:PVC:Z0, b) PANI:PVC:Z1, c) PANI:PVC:Z2, d) PANI:PVC:Z3, e) PANI:PVC:Z4 and PANI:PVC:Z5 under cyclic ageing conditions

surface morphology of HCl (1M) doped nanocomposite PANI:PVC:Z5 totally different and flaky. From the surface observation, it may be assumed that HCl would have reacted with ZnO nanoparticles in the nanocomposite while doping, consequently, changing the surface appearance rough. It can also be suggested that the ZnO nanoparticles have played a significant role in decreasing the electrical conductivity of the nanocomposites. Transmission Electron Microscopy (TEM) micrographs of ZnO nanoparticles and PANI:PVC:Z5 nanocomposite (Fig. 7) confirms that the particles zinc oxide nanoparticles and that of nanocomposites are within the nano range. Therefore, it may be suggested that the technique used for the preparation of PANI and PANI:PVC:Z5 nanocomposite are very promising for the preparation of other nanocomposites<sup>2</sup>.

### XRD studies

The diffraction patterns of the ZnO nanoparticles and PANI:PVC:Z5 nanocomposite powders were obtained by scanning these samples at an interval of  $2\theta = 0-60^\circ @ 2^\circ/\text{min}$ . Peaks obtained for pure zinc oxide nanoparticles ( $2\theta = 31.8340, 34.4853, 36.3303, 47.6017$  and  $2\theta = 56.6575$ )<sup>27</sup> are also present in each of the nanocomposites PANI:PVC:Z5 ( $2\theta = 31.8251, 34.4851, 36.2975, 47.5955,$

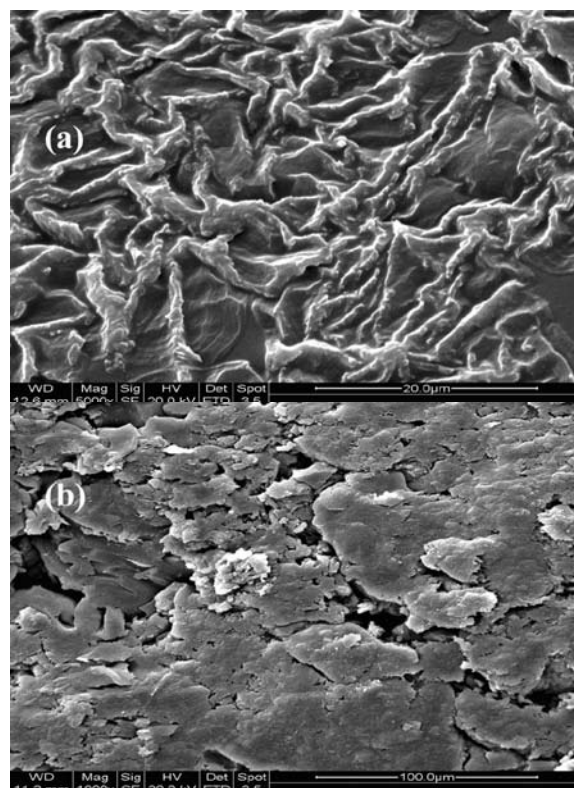


**Figure 6:** SEM micrographs of surface of a) undoped PANI film<sup>16</sup> and b) HCl doped PANI:PVC:Z5 film.

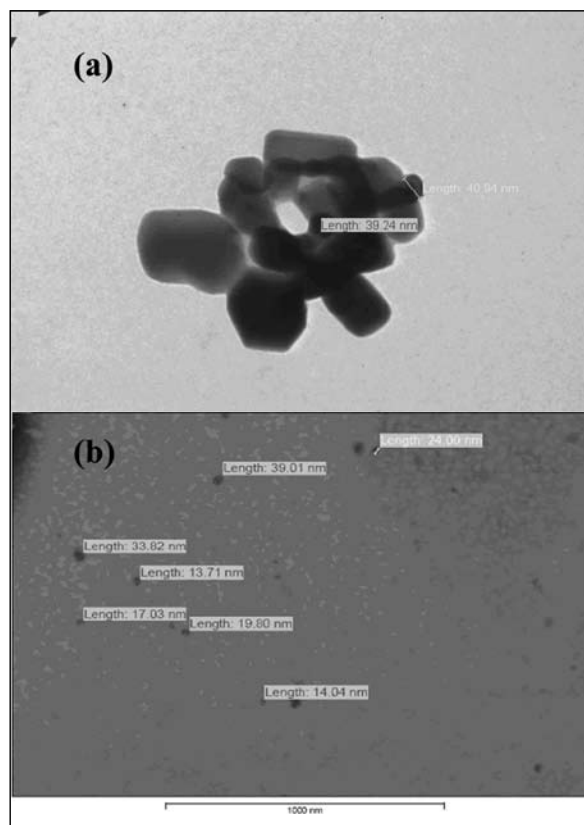


**Figure 7:** TEM micrographs of a) ZnO nanoparticles and b) PANI:PVC:Z5 nanocomposite.

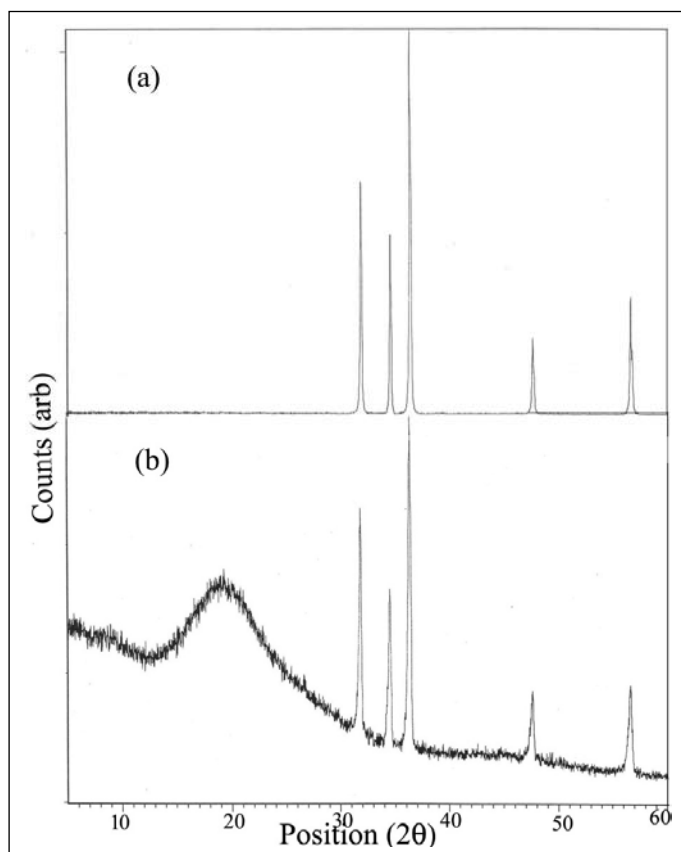


**Figure 8:** XRD diffractogram of a) ZnO nanoparticles<sup>16</sup> and b) PANI:PVC:Z5 nanocomposite

$2\theta=56.6283$ . XRD diffractogram of zinc oxide nanoparticles and that of PANI:PVC:Z5 nanocomposites similar peak patterns, thereupon, it may be assumed that there was no structural change in ZnO in presence of polyaniline or negligible change which might be ignored. These results also indicate toward the amorphous nature of the polyaniline present in nanocomposites. Moreover, it might also be suggested that supporting polymer into nanocomposite does not affect the crystal structure of zinc oxide nanoparticles. However, little decrease in size of ZnO nanoparticles were observed due to the formation of Zn-polymer complex on the surface of ZnO nanoparticles<sup>8,28</sup>.

### Conclusions

In the present work, we have successfully prepared organic-inorganic conducting nanocomposites of PANI with ZnO nanoparticles and PVC as supporting matrix. All conducting nanocomposites were characterized for their electrical properties and selected samples were characterized using FTIR, SEM, TEM and XRD. The electrical conductivity of the conducting nanocomposites was found to be fairly good and all the nanocomposites showed semiconducting behavior when doped with HCl. ZnO nanoparticles played significant role in the nano-

composite, while behaving as dedoping agent for PANI it also stabilized the electrical conductivity in term of retention. The thermooxidative stability as well as stability in terms of dc electrical conductivity retention was found to be good for all nanocomposites, therefore, their use in sensors, battery and electronic applications below 100°C is suggested.

### Acknowledgements

Authors are thankful to instrumentation facility of department of chemistry of AMU, Aligarh for FTIR analysis, SAIF (AIIMS, New Delhi) for TEM facility, SAIF (Punjab university Chandigarh) for XRD studies, Prof. Faiz Ahmad Khan for providing SEM images of samples and the University Grant Commission (India) for providing financial support.

### References

1. M. O. Ansari, M. M. Khan, S.A. Ansari, K. Raju, J. Lee and M.H. Cho, *ACS Appl. Mater. Interface*, **2014**, *6*, 8124.
2. S. P. Ansari, F. Mohammad, *ISRN Mater. Sci.*, **2012**, *2012*, ID 129869, 1-7.
3. X. Lei, Z. Su, *Polym. Adv. Technol.*, **2007**, *18*, 472.
4. L. S. Schadler, *Nanocomposite Science and Technology*, WILEY-VCH Weinheim 2003.
5. M. O. Ansari, S. P. Ansari, S. K. Yadav, T. Anwer, M. H. Cho, F. Mohammad, *J. Ind. Eng. Chem.*, **2014**, *20*, 2010.
6. M. O. Ansari, M. M. Khan, S.A. Ansari, I. Amal, J. Lee and M.H. Cho, *Materials Letter*, **2014**, *114*, 159.
7. A. A. Ahmed, F. Mohammad and M.Z.A. Rahman M. Z.A., *J. Appl. Polym. Sci.*, **2006**, *99*, 437.
8. Y. He, *Appl. Surf. Sci.*, **2005**, *249*, 1.
9. Z. S. Seddigi, S. A. Ahmed, S. P. Ansari, N. H. Yarkandi, E. Danish, A. A. Alkibash, S. Ahmed, *Photochem. Photobiol.*, **2014**, *90*, 491.
10. H. Mekki, M. Belbachi, *eXP. Polym. Letts*, **2007**, *1*, 495.
11. R. F. De Farias, L. M. Nunes, *J. Thermal Anal. Calorimetry*, **2002**, *70*, 559.
12. S. Rajendran, M. Ramesh Prabhu, M. Usha Rani, *Int. J. Electrochem. Sci.*, **2008**, *3*, 282.
13. V. Singh, S. Mohan, G. Singh, P.C. Pandey, R. Prakash, *Sens. Actuat. B*, **2008**, *132*, 99.
14. S. P. Ansari, F. Mohammad, *Iran. Polym. J.*, **2016**, *25*, 363.
15. S. P. Ansari, F. Mohammad, *Polymer and Polymer Composites*, **2016**, *24*, 273.

16. S. P. Ansari, F. Mohammad, *The IUP J. Chem.* **2010**, III, 7.
17. M. G. Han, S. K. Cho, S. G. Oh, S. S. Im, *Synth. Met.*, **2002**, 126, 53.
18. A. An`lovar, Z. C. Orel, M. Zigon, *Polimeri*, **2008**, 29, 84-87
19. N.V. Blinova, J. Stejkal, M. Trchova, J. Prokes and M. Omatsova, *Eur. Polym. J.*, **2007**, 43, 2331.
20. X.B. Yan, Z.J. Han, Y. Yang, B.K. Tay, *Sens. Actuat. B*, **2007**, 123, 107.
21. A. A. Ahmed, F. Mohammad, M. Z. A. Rahman, *Synth. Met.*, **2004**, 144, 29.
22. A. Olad and A. Rashidzadeh, *Iran. J. Chem. Engg.*, **2008**, 5, 45.
23. Y. Tan, Y. Zhang, J. Kan, *Exp. Polym. Lett.*, **2009**, 3, 333.
24. M. S. Khan, R. A Qazi, M. S. Wahid, *African J. Pure and Appl. Chem.*, **2008**, 2, 41.
25. Y. M. Lee, J. H. Kim, J. S. Kang, S. Y. Ha, *Macromolecules*, **2000**, 33, 7431.
26. J. Anand, P. S. Rao, S. Palanipappan, D.N. Sathyanarayana, *Synth. Met.* **1998**, 95, 57.
27. L.P. Bauermann, A. d. Campo, J. Bill, F. Aldinger, *Chem. Mater.*, **2006**, 18, 2016.
28. E. Tang, G. Cheng, X. Maa, X. Pang, Q. Zhao, *Appl. Surf. Sci.*, **2006**, 252, 5227.

# Strategic design of gold nanoparticles for the complete elimination of tumour cells: Potential and challenges

Manu Lopus\*

*School of Biological Sciences, UM-DAE Centre for Excellence in Basic Sciences, Mumbai-400098, India*

Man's fascination with gold started several millennia ago for its ornamental value and rarity. In addition, gold has long been known for its medicinal properties. Gold powder (Swarna bhasma), for example, has been used in many Ayurvedic formulations. With the advent of nanotechnology, this precious metal has been investigated extensively for its therapeutic value. Interest in gold nanoparticles as potential anticancer agents began approximately a decade ago when researchers found that tumour architecture causes nanoparticles to preferentially accumulate at the tumour site. The propensity of gold nanoparticles to target tumours due to their "enhanced permeability and retention" (EPR effect) at the tumour sites makes them potential cancer therapeutics (1). Specifically, unlike normal tissues, tumour tissues and their immediate vicinity have leaky blood vessels and compromised lymphatic clearing system. Although it cannot be asserted conclusively, the EPR effect is thought to enable size-optimized nanoparticles to retain at these sites to exert their effects. While the anticancer potential of gold nanoparticles is known (2), their intracellular targets and details and manifestations of their interactions with these targets are poorly understood.

## Tubulin and Microtubules

Tubulin is a protein that builds the cytoskeletal filament, the microtubule, through its GTP- and temperature-dependent, reversible addition. The assembly dynamics of microtubules play vital roles in several cellular processes including positioning of cellular organelles, transportation of cellular cargoes, and provision of structural stability to cells (3). When a cell is about to divide into two, the microtubules undergo a dramatic reorganization to form the "mitotic spindle." The spindle then orchestrates accurate separation of duplicated chromosomes to the newly-forming daughter cells. The division cycle of eukaryote cells comprises four stages, namely, G1 phase, S-phase, G2 phase, and mitosis. During G1, the cell synthesizes proteins required for DNA duplication, and it also grows. In S-phase, the chromosomes duplicate. From S-phase, the cell progresses to the G2 phase where a final check for the intactness of duplicated chromosomes will be done, and the cell would grow further in preparation for its division into two cells. The cell then enters mitosis where the segregation of chromosomes happens. Finally, cytokinesis, the actual division of the cell, happens. After

the division, depending on the need, the cell may either start a next cycle of division or enter a resting phase called G0.

Since microtubules play crucial roles in cell division, they have also formed an attractive target for cancer chemotherapy. From the classic drugs, such as taxol and vinblastine, to the latest ones including Ixempra, and Halaven, these drug molecules interact with tubulin and microtubules in a multitude of ways and alter their natural assembly dynamics (4, 5). The deviated/suppressed dynamicity of the microtubules then brings forth a plethora of cellular responses: if the cell's effort to survive fails, it dies in a programmatic manner; coordinated by a variety of proteins that exist in cells almost exclusively to execute this programmed death. Although the concept of inducing cancer-specific cell death appears appealing and its implementation effective, there remain multiple challenges to overcome for efficacious cancer therapy. The challenges include drug resistance, target specificity, and severe side effects- to name a few.

## Gold nanoparticles as tubulin-targeted agents

Although not studied extensively, we have some information on the interactions between gold nanoparticles and tubulin. For example, using Raman and Fourier transform-infrared (FTIR) spectroscopies, Choudhuri and colleagues showed the ability of gold nanoparticles to perturb structural integrity of tubulin, leading eventually to inhibition of tubulin assembly (6). Further, using a combination of darkfield microscopy, hyper spectral imaging, and confocal laser scanning microscopy, it was further demonstrated that the particles are capable of inducing aggregation of microtubules in cancer cells (6).

Tumour specificity and complete elimination of tumour cells which are in different phases of their division cycle are major challenges associated with the therapeutic intervention of cancer. Given the above insights, we investigated whether gold nanoparticles can be used as potent antitumour agents that can disrupt cell cycle progression in cancer cells. A recent study published from our laboratory (7) showed a tubulin-targeted antiproliferative mechanism of action of tryptone-stabilized gold nanoparticles (TsAuNPs). For this study, we synthesized TsAuNPs using  $\text{HAuCl}_4 \cdot 3\text{H}_2\text{O}$  and tryptone through microwave irradiation. After characterizing the

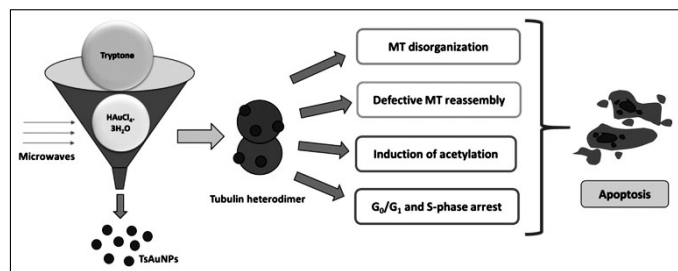


**Figure 1.** The synthesis, and a potential, tubulin-targeted mechanism of action of Ts-AuNPs (7). The binding of Ts-AuNPs to tubulin disruptively interfered with the microtubule network in cells, induced suboptimal reassembly of the microtubules, and altered the normal dynamicity of microtubules (7). The treated cells eventually underwent programmed cell death (apoptosis)

particles by a variety of spectroscopic methods, including UV-visible spectrophotometry, Fourier-transform infrared spectroscopy, X-ray diffraction, DLS-Zeta potential, and transmission electron microscopy enabled with energy-dispersive X-ray spectroscopy, we evaluated the anticancer potential of these particles in established cancer cell lines. Specifically, we the particles inhibitory to the viability of human pancreatic (PANC-1), cervical (HeLa), and breast (MDA-MB-231) cancer cell lines in a concentration-dependent manner, with the highest efficacy against PANC-1 cells and that the particles can strongly suppress the clonogenic propensity of PANC-1 cells (cancer oftentimes propagates in the body by making new colonies). The particles competitively inhibited anilinonaphthalene sulfonate (ANS) binding to tubulin, indicating, indicating direct binding of the particles to tubulin. Polymer mass analyses of microtubules formed in the presence of the particles revealed suppression of tubulin assembly. Investigating the trans cellular manifestation of these nanoparticles, it was found that TsAuNPs-mediated inhibition of cell viability involves an unusual mode of differential cell cycle arrest (arrest at both  $G_0$ - $G_1$  phase and S-phase) followed by apoptosis(7). For tubulin interacting agents, this is an unusual observation. Antitubulin agents in general arrest cells at one phase, mostly  $G_2$ /M or at the spindle assembly stage (4). Nevertheless, there are tubulin-targeted agents that arrest cells outside mitosis as well, and include drug such as beta-lapachone that arrests cells in S-phase (8). Immunofluorescence imaging of cells treated

with the particles revealed disrupted microtubule network, and defective re-polymerization of cold-disassembled microtubules. Further, the particles appeared to interfere with the dynamicity of microtubules as evidenced by an apparent enhancement of tubulin acetylation (7). These findings suggest that TsAuNPs hold considerable anticancer potential. For example, tumor-specific delivery of TsAuNPs in combination with a  $G_2$ -M blocker may enhance elimination of cancer cells which are in different phases of cell cycle.

### Future Perspective

There is a long way to go before bringing this idea to the market. There are several challenges to overcome. The size of the nanoparticles, for example, needs to be optimized for their desired retention at the site of tumour, and low toxicity to normal tissues and organs. The particles require smart delivery through novel methods such as liposomal encapsulation or antibody conjugation. Successful delivery and realization of tumor regression in animal models would further scrutinize their efficacy as drug molecules. The fine details of their working in cancer cells and their potential toxicities need thorough examination. The formulation must then survive extensive preclinical studies and different stages of clinical evaluation to get clinical approval.

### Acknowledgment

The author thanks UM-DAE Centre for Excellence in Basic Sciences for the financial support.

### References

1. Wang J, et al., *Curr Drug Metab.* **2010**, 11, 129-41
2. He C, Lu J, Lin W. *J Control Release.* **2015** 219, 224-236
3. Lopus M, Yenjerla M, and Wilson L. *In Wiley Encyclopedia of Chemical Biology*, Begley TP, Ed. Wiley, NJ. **2009**, 3, 153-160
4. Dumontet C, Jordan MA. *Nat Rev Drug Discov.* **2010**, 9, 790-803
5. Mahaddalkar T and Lopus M. *Curr Topic Med Chem*, **2017**, 17, 2559-2568
6. Choudhury D, Xavier PL, Chaudhari K, John R, Dasgupta AK, Pradeep T, Chakrabarti G. *Nanoscale.*2013, 5, 4476-89
7. Mahaddalkar T, et al., (2017) *Exp Cell Res*, 360, 163-170
8. Y. Li, X. Sun, J.T. LaMont, A.B. Pardee, C.J. Li, *Proc Natl AcadSci USA*, **2003**, 100, 2674-2678.



**Dr. Manu Lopus** is a Reader in Biology at UM-DAE Centre for Excellence in Basic Sciences, Mumbai. He received a Ph.D. in Biotechnology at Indian Institute of Technology Bombay under the guidance of Prof. Dulal Panda. He completed his postdoctoral training at the department of molecular, cellular, and developmental biology, University of California, Santa Barbara, in the laboratories of Prof. Leslie Wilson and Dr. Mary Ann Jordan. Dr. Lopus is a Life Member of the National Academy of Sciences, India.

## Effects of antioxidants melatonin and glutathione on human serum albumin aggregation: biophysical studies

Vikas Kumar<sup>1</sup>, Ramakrishna V. Hosur<sup>2</sup> and Sinjan Choudhary<sup>1</sup>

<sup>1</sup>School of Chemical Sciences, UM-DAE Centre for Excellence in Basic Sciences, University of Mumbai, Kalina, Santacruz (E) Mumbai 400098, India.

<sup>2</sup>Department of Chemical Sciences, Tata Institute of Fundamental Research, Homi Bhabha Road, Mumbai 400005, India.

### Abstract

Protein aggregation is a major source of disorders in living systems and all efforts to prevent such phenomena are most welcome. In this context, we have characterized and quantified here the effects of melatonin and glutathione, two major antioxidants in blood plasma, on the aggregation of human serum albumin (HSA), an important transport protein. Thioflavin T (ThT) binding assays were performed to study effects of melatonin/glutathione on HSA aggregation kinetics. Transmission electron microscopy (TEM) is used for monitor morphological features of the aggregates formed. The values of limiting enthalpies of interaction ( $\Delta H_{\text{lim}}^0$ ) for melatonin and glutathione with HSA at various stages of fibrillation process were determined by using isothermal titration calorimetry (ITC). ThT binding assay suggests that melatonin is very effective against HSA aggregation as it causes delay in the onset of aggregation and decrease in extent of aggregation in a concentration dependent manner. The values of ( $\Delta H_{\text{lim}}^0$ ) for melatonin and glutathione suggests that a combination of polar as well as hydrophobic interactions is responsible for inhibition of HSA aggregation. TEM images show presence of large aggregates of HSA which reduce in presence of melatonin. These observations have significant biological implications, since HSA is the main transport protein present in the blood and its aggregation would adversely affect its transport capability which could lead to metabolic disorder. Our results indicate that any suitably designed drug which mimic melatonin or which can enhance melatonin production inside the body would have significant therapeutic value against HSA aggregation borne diseases.

**Key words:** Antioxidants, inhibitors, aggregation, interaction, inhibition.

### Introduction

Proteins are the most important molecules for life and perform varieties of function when they are in the native state. But when proteins undergo misfolding/unfolding and aggregation under stressful conditions and form amyloid fibrils, it leads to various diseases such as Alzheimer, Parkinson, diabetes II, Huntington, etc.<sup>1-5</sup> In view of these implications, considerable efforts have been devoted to understand the fibrillation process of proteins and then to screen the compounds that have ability to interfere with the same.<sup>6-7</sup>

Human serum albumin (HSA) is a globular protein which contains 585 amino acids and 17 disulfide bonds.<sup>8,9</sup> It is composed of three structurally similar domains (I, II and III) and each contains two sub-domains (A and B).<sup>10</sup> HSA is the most abundant serum protein in human, exhibits multifunctional transport properties by binding to a large number of drugs and other molecule like fatty acids, hormones etc.<sup>11-14</sup> Apart from binding and transport properties, HSA is involved in many other functions, like maintaining pH, osmotic pressure.<sup>15</sup> It prevents photodegradation of folic acid and is a marker of an

inflammatory state.<sup>16</sup> Although HSA is a stable protein, it is susceptible to undergo aggregation under certain external conditions.<sup>17, 18</sup> HSA is known to form amyloid like aggregates at elevated temperatures and in presence of organic solvents at physiological pH 7.4.<sup>19-21</sup> It is also reported that HSA aggregates show self-seeding feature and any amyloid contamination may induce risk factor for initiation of in vivo HSA aggregation.<sup>22</sup> With this view we have studied here aggregation and amyloid formation of HSA. In addition to its importance as drug carrier, a lot of work has been done recently on inhibition of HSA aggregation in vitro with an aim of designing drugs which can prevent HSA aggregation.<sup>23-24</sup> Prevention of HSA aggregation is not only important for its therapeutic use but it can also shed light on fibrillation mechanism in general and its prevention in similar proteins.

Many small molecules like polyphenols, vitamins, nucleotides, synthetic peptides and antioxidants have been reported to inhibit protein aggregation.<sup>25, 26</sup> In general, a small fraction (less than 5%) of oxygen intake by cell gets converted into reactive oxygen species like  $O_2^-$ ,  $H_2O_2$ ,  $O_2$  and  $OH^-$  radicals, which are toxic in nature and if allowed

to accumulate can lead to oxidative stress and destroy macromolecules of the cell.<sup>27</sup> Exposure of HSA to oxidative environments could significantly affect its conformation, hence its biological function. Oxidatively modified forms of HSA which include aggregated species under oxidative stressed conditions have indeed been detected in a number of pathological conditions.<sup>28</sup> Anti-oxidants are known to prevent conversion of normal oxygen into reactive oxygen species like  $O^{2-}$ ,  $H_2O_2$ ,  $O_2$  and  $OH\cdot$  radicals. Some of the recent reports suggest that antioxidants such as diallylsulfide, vanillin, resveratrol, curcumin etc. have ability to inhibit and modulate HSA aggregation.<sup>29-32</sup>

Melatonin is a small molecule found in animals and plants. It is basically a hormone, secreted from pineal gland in all vertebrates including humans and has anti-oxidant properties.<sup>33</sup> In plants, it functions as a first line of defence against oxidative stress.<sup>34</sup> Melatonin has been reported to have remarkable anti-oxidant properties by acting as both free radical scavenger and preventive antioxidant.<sup>35-37</sup> It also regulates sleep, jet lag, shift-work disorder, sleep-wake fullness rhythm, and seasonal affective disorder.<sup>38</sup> Melatonin has been reported to enhance the synthesis of antioxidative enzymes like superoxide dismutases<sup>40</sup> which is involved in prevention of conversion of normal oxygen into reactive oxygen species like  $O^{2-}$ ,  $H_2O_2$ ,  $O_2$  and  $OH\cdot$  radicals.

Glutathione (GSH) is a tri-peptide consisting of glycine, cysteine and glutamic acid. It plays an important role in cellular homeostasis.<sup>41</sup> It is a ubiquitous molecule that is produced in all organs, especially in the liver and is present in almost all mammalian tissues.<sup>42</sup> GSH reduces disulphide bonds acting as electron donor, and in this process it gets converted into its oxidized form glutathione disulphide (GSSH) also called L(-)-glutathione.<sup>43</sup> In humans, GSH is involved in various physiological functions such as detoxification of xenobiotics (drugs, pollutants and carcinogens) in cells. GSH is both a nucleophile and reductant, hence reacts with electrophiles or oxidizing species before they interact with critical cellular components like nucleic acid and proteins.<sup>41, 42</sup> Other important physiological function of GSH is to maintain integrity of red blood cell and it acts as an important cofactor in many biological functions like catabolism, transport and metabolism.<sup>42-44</sup> In a healthy living cell, more than 90% of glutathione is found in reduced form (GSH) while less than 10% as oxidized form (GSSH). However, pathological conditions causing oxidative stress leads to conversion of GSH into GSSH.<sup>44, 45</sup> The ratio of GSH and GSSH in the cell is often used to measure cellular toxicity.<sup>46</sup>

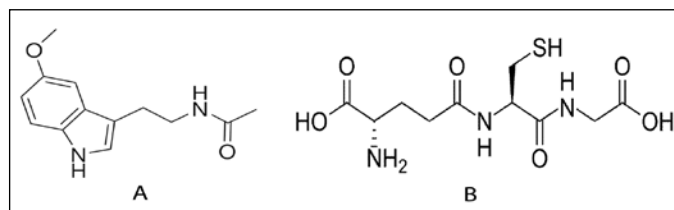


Fig 1. Chemical structures of (A) melatonin and (B) glutathione.

Melatonin and glutathione are the major antioxidants present in the blood plasma and act as a primary defence against free radical attack.<sup>47, 48</sup> The chemical structures of these molecules are shown in Fig.1.

It has also been reported in literature that melatonin is many times superior than glutathione (GSH) in scavenging reactive radicals.<sup>49</sup> Normal level and rate of production of melatonin is important in preventing age-associated degenerative changes occurring in cells and tissues of the body.<sup>50</sup> Since production of melatonin decreases with age, it leads to increased level of oxidative stress and associated degenerative changes like Alzheimer and Parkinson disease, seen in old age.<sup>51</sup> In the present work we have demonstrated an additional possible functional role for the two compounds, namely, inhibitory effect of melatonin and L-glutathione on human serum albumin (HSA) aggregation at physiological pH (pH 7.4) by employing a combination of spectroscopic, calorimetric, and microscopic techniques. We have also gained insight into the mode of interaction of these molecules with HSA at different stages of aggregation which can eventually help in design and development of appropriate inhibitors/drugs of protein aggregation phenomenon, in general.

## Materials and Methods

### Materials

Human serum albumin (HSA), L-glutathione reduced, melatonin and thioflavin-T (ThT) and sodium chloride (NaCl) were obtained from Sigma-Aldrich Chemicals Company (USA). All the reagents were of analytical grade and were used without further purification. HSA, glutathione and melatonin were dissolved in phosphate buffer saline (PBS) (5 mM, pH 7.4 and NaCl 0.1 M). Stock solutions of glutathione and melatonin were prepared and used immediately to avoid oxidation under light and air. ThT stock solution (5 mM) was prepared in phosphate buffer solution at pH 7.4.

### Absorbance measurements

HSA and ThT concentrations were determined on spectrophotometer (Jasco) using extinction coefficients  $\epsilon_{280} = 35,700 \text{ mol}^{-1} \text{ L cm}^{-1}$ <sup>52</sup> and  $E = 26,620 \text{ mol}^{-1} \text{ L cm}^{-1}$ ,<sup>53</sup> respectively with 1.0 cm quartz cells at 298K. PBS and

phosphate buffer solutions were used as reference for determining of concentrations of HSA and ThT respectively.

### In-vitro HSA fibrillation

HSA stock solutions were prepared in 5 mM phosphate buffer saline (pH 7.0) in presence of 150 mM NaCl. In order to induce fibrillation, 160  $\mu$ M HSA was incubated at 50 °C at a stirring rate of 250 rpm.

### ThT binding kinetics

HSA fibrillation kinetics was monitored by studying the binding of thioflavin T on a Cary Eclipse fluorescence spectrophotometer. Thioflavin T (ThT) is a cationic benzothiazol dye which is used to detect amyloid formation. Upon selective excitation at 450 nm, it gives characteristic maxima at 480 nm upon with fibrillar aggregates. Excitation and emission slit widths were fixed at 5 nm each.

A stock solution of ThT was prepared in phosphate buffer (5mM, pH 7.0). At different time intervals an aliquot of incubated sample solution was mixed with ThT solution such that the final concentrations of protein and ThT in the fluorescence measurements were 5  $\mu$ M and 50  $\mu$ M, respectively. The samples were excited at 450 nm and emission was detected at 482 nm.<sup>54</sup> The acquired data from ThT fluorescence measurements were fitted to the sigmoid curve represented by the following equation<sup>55</sup>

$$Y = y_i + m_i x + \frac{y_f + m_f x}{1 + e^{-(t-t_0)/\tau}} \quad (1)$$

Here  $Y$  is the fluorescence intensity,  $t$  is time, and  $t_0$  is the time to reach 50% of maximal fluorescence. Thus, the apparent rate constant,  $k_{app}$ , for the growth of fibrils is given by  $1/\tau$ , and the lag time is given by  $t_0 - 2\tau$ , where  $\tau$  is the time constant of fibril growth and obtained by nonlinear regression. Each experiment was performed at least three times and an average was used to report the final result. The reported fluorescence emission spectra of the HSA-ThT complexes were corrected by subtracting the reference spectra of the control solutions containing same amount of the dye.

### Transmission electron microscopy

The visualization of the HSA aggregates was done on a JEOL JEM-2100 Electron Microscope which operates at an accelerating voltage of 200 kV. The TEM samples were prepared by depositing 10  $\mu$ L of fibril sample diluted 20 times in filtered buffer on Formvar-coated 75 mesh copper grids. The negative staining of the TEM samples were done with 2% aqueous uranyl acetate solution which is known

to produce high electron density and image contrast as well as impart fine grain to the image.<sup>56</sup> A 0.22 mm filter was used to filter the stains. The grids were rinsed with large volumes of water and dried in air before examined to acquire images.

### Isothermal Titration Calorimetry

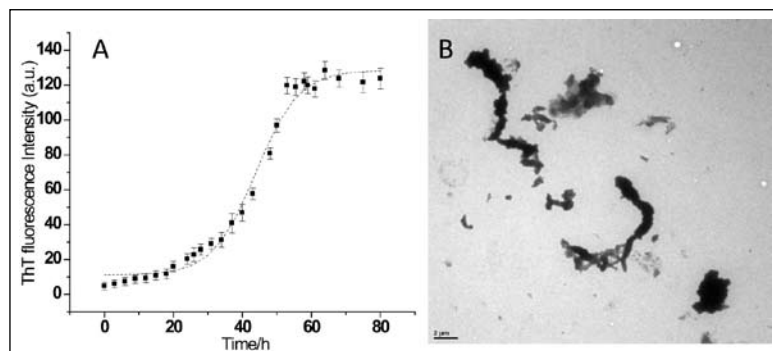
The interactions of HSA aggregates with melatonin and glutathione were studied by using a VP isothermal titration calorimeter (Microcal LLC Northampton MA). Experiments were carried out by titrating HSA at native and different stages of fibrillation into the sample cell containing buffer or appropriate amount of the melatonin/glutathione in aliquots using a rotating stirrer-syringe of 250  $\mu$ l capacity. The reference cell was filled with the respective buffer. The isothermal titration calorimetric (ITC) experiments were designed for a total of 10 consecutive injections, each having a volume of 10  $\mu$ l of 0.160 mM native HSA solution or heat induced fibril solution into buffer or different concentrations of melatonin/glutathione solution in the cell. The duration between consecutive injections was 10 s with an interval of 4 min between each injection. The heats of dilutions were measured by titrating buffer with melatonin/glutathione at the same concentrations and procedure as used in the main experiments. All the ITC profiles were dilution corrected before analysis to determine the heat of interaction by using Origin 7.0 software supplied by Microcal.

## Results and discussion

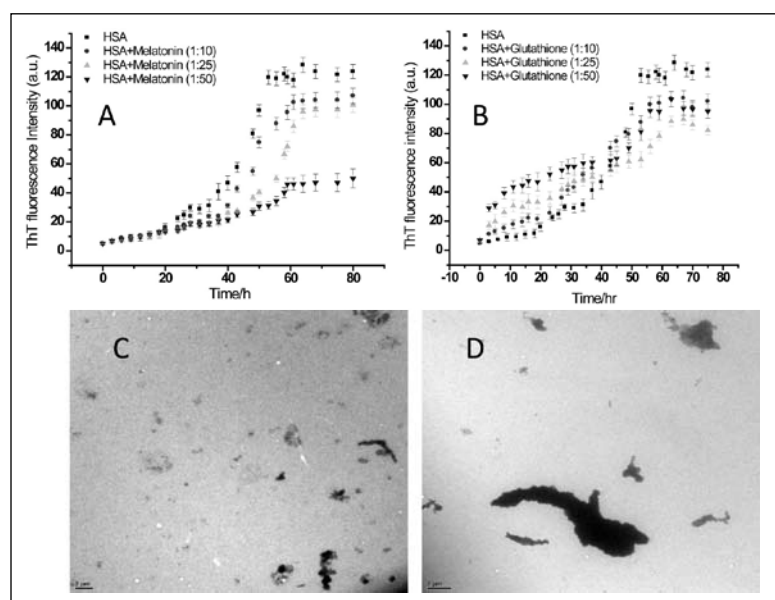
### Human serum albumin aggregation

Fig. 2 shows the time course of aggregation of 160  $\mu$ M HSA prepared in 5 mM phosphate buffer saline (PBS) at pH 7.4 having 0.2 M NaCl. The sample was incubated at 50 °C at stirring rate of 250 rpm. The ThT binding assay was performed to monitor HSA fibril extension. The fibrillation curve for aggregation of HSA shows sigmoidal behaviour consisting of three distinct phases; initial lag phase which is quite long, a subsequent elongation phase and a final saturation phase (see Fig. 2A).

The lag time for HSA fibrillation calculated by using equation (1) is found to be (32.39 $\pm$ 1.1) h. In order to further confirm the HSA fibrillation independently, transmission electron microscopy (TEM) was performed. Fig. 2B shows the TEM image of HSA aggregates taken after 72 h of incubation. It is clear from the figure that under the studied experimental conditions HSA has formed bundle of aggregates. HSA is known to form aggregates which display variable morphologies under varying aggregation conditions.<sup>57</sup> The possible reason for this could be the formation of different structural intermediates during the



**Fig 2.** (A) Kinetics of the HSA amyloid aggregation monitored by ThT binding assay, and (B) transmission electron microscopic (TEM) images of HSA aggregates after 72 h of incubation.



**Fig 3.** Kinetics of HSA aggregation in the absence and presence of different concentration of (A) melatonin and (B) glutathione monitored by ThT binding assay, and TEM images of HSA aggregates after 72 h of incubation in presence of (C) melatonin and (D) glutathione at [HSA]/[Melatonin or glutathione] 1:50.

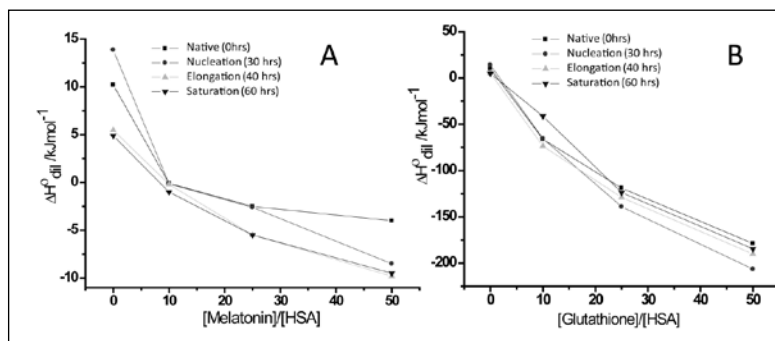


**Fig 4.** Limiting standard enthalpies of interaction of HSA with (A) melatonin and (B) glutathione at different stages of HSA aggregation.

HSA aggregation pathway.<sup>57</sup> Since the aggregates formed under the present aggregation conditions show appreciable enhancement of ThT fluorescence, presence of  $\beta$ -structure is indicated. Thus these bundle of aggregates may also be consisting of small fibrillar structures.

### Effects of melatonin and L-glutathione on HSA fibril formation

In order to check the effects of melatonin and L-glutathione on HSA aggregation, kinetics of ThT binding experiments in absence and presence of different concentrations of melatonin and L-glutathione were studied. The concentration of HSA in these experiments was 160  $\mu$ M and [HSA]/[melatonin or glutathione] molar ratios were maintained as 1:10, 1:25 and 1:50 in different experiments. Fig. 3A shows the time course of aggregation of HSA in absence and presence of different concentrations of melatonin.

In presence of melatonin at [HSA]/[Melatonin] molar ratio 1:10, there is an increase in lag period of HSA aggregation to  $(35.8 \pm 0.6)$  h. Further increase in the molar ratio of [HSA]/[Melatonin] to 1:25, lag time becomes  $(44.1 \pm 0.6)$  h with a decrease in the ThT fluorescence intensity. The ThT fluorescence intensity continues to decrease when [HSA]/[Melatonin] ratio is further increased to 1:50. Here, increase in the inhibition of HSA aggregation by melatonin is clearly reflected in terms of decrease in ThT fluorescence intensity.

On the other hand when the ThT kinetics studies were performed at [HSA]/[Glutathione] molar ratio of 1:10, the lag time decreased to  $[(16.1 \pm 0.6)$  h] compared to that in the absence of Glutathione. Although the final ThT fluorescence intensities are slightly less at higher molar ratios of [HSA]/[Glutathione] compared to that in absence of glutathione, glutathione has induced onset of aggregation at the very early stages of fibrillation (see Fig. 3B). The ThT binding results clearly demonstrate that even though both melatonin and glutathione are responsible for antioxidative properties of the cell, their ability to inhibit aggregation is very different. Fig. 3C and D show the TEM images of HSA in presence of melatonin and glutathione (1:50) after 72 h of incubation. It is evident from the figure that aggregation is reduced in the presence of melatonin. On the other hand a mixture of large and small aggregates was observed

in presence of glutathione. The TEM images suggest that melatonin suppresses aggregation of HSA whereas glutathione is relatively less effective.

### Thermodynamics of protein aggregation

Protein fibrillation is accompanied by large conformational changes in which protein molecules have different extents of hydrophobic and hydrophilic groups exposed to the solvent medium. The molecular properties of the protein and inhibitor are responsible for interactions involved and hence to the extent of inhibition of fibrillation. In order to understand the differential abilities of melatonin and glutathione in fibrillation inhibition, it is very important to understand the types of interactions involved between melatonin/glutathione and HSA at different stages of fibrillation. To understand the mode of interactions of melatonin and glutathione with HSA, isothermal titration calorimetry (ITC) experiments were performed at different stages of fibrillation. ITC is a widely accepted technique for characterization of intermolecular interaction and is highly sensitive to detect small amounts of heat changes. Depending upon the nature of the reaction (either exothermic or endothermic reaction) ITC measures the heat released or absorbed by gradual addition of ligand to the macromolecular solution. At equilibrium, the standard Gibbs free energy of binding ( $\Delta G^\circ$ ) at a temperature T is governed by standard enthalpic ( $\Delta H^\circ$ ) and entropic ( $\Delta S^\circ$ ) changes, and are expressed by following equation:

$$\Delta G^\circ = \Delta H^\circ - T\Delta S^\circ \quad (2)$$

The change in standard Gibbs free energy of the system should be negative for spontaneous binding of a ligand to a protein.<sup>58</sup> The sign and magnitude of  $\Delta G^\circ$  depend on the thermodynamic quantities  $\Delta H^\circ$  (heat change) and  $\Delta S^\circ$  (change in randomness of the system), which are the main driving forces for protein ligand binding. The binding enthalpy ( $\Delta H^\circ$ ) represents heat evolved or absorbed resulting from the formation of various noncovalent interactions in the interacting system.<sup>59</sup>

The ITC experiments were performed with HSA in presence of melatonin and glutathione at native stage and at different stages of fibrillation. In all the ITC experiments the concentration of HSA solution taken in the syringe was 0.160 mM. Melatonin/glutathione solutions were taken inside sample cell at different concentrations (1.60, 4.0 and 80.0 mM). The ITC profiles for interaction of melatonin and glutathione with HSA do not follow a typical binding profile leading to saturation level, but do show an interaction pattern. Fig. 4 represents limiting standard enthalpy of interaction ( $\Delta H_{lim}^0$ ) of HSA at different stages of fibrillation in presence and absence of

different concentrations of melatonin and glutathione. The limiting standard enthalpy of interaction ( $\Delta H_{lim}^0$ ) which is indicative of nature of solute-solvent interactions was calculated by fitting a linear equation to the experimental data points. Fig. 4A and B represent the values of limiting standard enthalpies of interactions ( $\Delta H_{lim}^0$ ) of HSA with melatonin and glutathione, respectively. The values of ( $\Delta H_{lim}^0$ ) for HSA in absence of melatonin and glutathione are endothermic ranging from  $(10.20 \pm 0.20)$  kJ mol<sup>-1</sup> to  $(4.92 \pm 0.08)$  kJ mol<sup>-1</sup> from native to fibrillar stages. This corresponds to heat of dilution of HSA in the buffer. Upon addition of melatonin at [Melatonin]/[HSA] molar ratio 10, the values of ( $\Delta H_{lim}^0$ ) become slightly exothermic. The small amount of exothermicity is attributed to the involvement of electrostatic/ionic interactions between HSA and melatonin.

With increase in the concentration of melatonin ([Melatonin]/[HSA] molar ratio of 25) the values of ( $\Delta H_{lim}^0$ ) become more exothermic, the extent of which increases with increase in the concentration of melatonin. This increase in exothermicity indicates strengthening of ionic/polar interactions between HSA and melatonin. In presence of glutathione (at [Glutathione]/[HSA] molar ratio of 10), the values of ( $\Delta H_{lim}^0$ ) are also exothermic varying from  $-(66.16 \pm 1.32)$  kJ mol<sup>-1</sup> to  $-(41.22 \pm 0.82)$  kJ mol<sup>-1</sup> when the protein is at different stages of aggregation/fibrillation. With further increase in the [Glutathione]/[HSA] molar ratio to 25, the values of ( $\Delta H_{lim}^0$ ) become more exothermic for interaction with the native  $-(118.90 \pm 2.36)$  kJ mol<sup>-1</sup>, nucleation  $-(139.04 \pm 2.78)$  kJ mol<sup>-1</sup>, elongation  $-(129.02 \pm 2.42)$  kJ mol<sup>-1</sup> and saturation  $-(123.80 \pm 2.48)$  kJ mol<sup>-1</sup> stages of HSA fibrillation. The value of exothermicity continues to increase when [Glutathione]/[HSA] molar ratio is increased to 50 where ( $\Delta H_{lim}^0$ ) becomes  $-(178.80 \pm 3.57)$  kJ mol<sup>-1</sup>,  $-(206.60 \pm 4.13)$  kJ mol<sup>-1</sup>,  $-(190.2 \pm 3.80)$  kJ mol<sup>-1</sup>, and  $-(184.6 \pm 3.62)$  kJ mol<sup>-1</sup> for interaction with the native, nucleation, elongation and saturation stages, respectively). Higher exothermic values of ( $\Delta H_{lim}^0$ ) suggest predominant contribution from ionic interactions. The values of exothermicity increase when native HSA is converted into partially folded states during nucleation and elongation stages at all the studied molar ratios of [Melatonin or Glutathione]/[HSA] (10, 25 and 50) followed by a decrease at saturation stage of the fibrillation. This can be rationalized in terms of less availability of exposed ionic groups of the side chains due to stacking of beta strands in the saturation stage.

Melatonin and glutathione possess different molecular properties. Presence of two rings and the groups like -NH-, -O-, -C=O in the molecular structure makes melatonin suitable to interact via hydrophobic as well as

ionic interactions. When a protein undergoes fibrillation process, first it becomes partially unfolded which makes hydrophobic and polar groups of proteins exposed to solvent medium. On the other hand hydrophobic interactions are the main driving force for aggregation. Thus a molecule which can interfere both in hydrophobic as well as polar interactions will be a better inhibitor compared to the molecules which can interact via either of the two components. The  $(\Delta H_{lim}^0)$  values of interaction of melatonin with HSA are slightly exothermic. This exothermicity denotes significant balancing of heat effects due to polar interactions by hydrophobic interactions which contribute towards endothermicity. The values of  $(\Delta H_{lim}^0)$  for interaction of HSA with glutathione are more exothermic compared to that with the melatonin. This is attributed to the presence of -NH, -SH and -COOH groups in glutathione which can interact via polar/electrostatic interactions. The inability of glutathione to inhibit the aggregation of HSA can be related to its inability to interact via hydrophobic interactions which are the main driving force for protein aggregation. Although both melatonin and glutathione are antioxidants, the results demonstrate that melatonin has greater ability to inhibit HSA fibrillation/aggregation.

Combining our results with the literature information it can be inferred that melatonin counters protein aggregation via two ways: first by directly interacting with protein and thus inhibiting its aggregation as discussed above and second by targeting other molecules which decrease stress level in body.<sup>40</sup> Thus, as melatonin is synthesized by body, any drug which enhances the production of melatonin, especially at old ages could be used for treatment of protein aggregation diseases.

## Conclusions

The present studies demonstrate a possible additional role as inhibitors of HSA aggregation in the blood plasma, for the naturally synthesized anti-oxidants, melatonin and glutathione, in the living systems. The ThT binding assays using fluorescence spectroscopy demonstrated formation of HSA aggregates and concentration dependent inhibitory effects of antioxidants melatonin and glutathione. Melatonin is observed to be stronger potent inhibitor of HSA aggregation than glutathione. The ITC data suggest that the large negative values of limiting enthalpy of interaction  $(\Delta H_{lim}^0)$  of glutathione with HSA is due to predominance of polar interactions whereas in case of melatonin the values are less. The relatively less negative values of limiting enthalpy of interaction  $(\Delta H_{lim}^0)$  in case of melatonin signify balancing of heat effects due to polar interactions by hydrophobic interactions which

contributes towards positive values. Thus, our ITC results suggest that a combination of polar as well as hydrophobic interactions is responsible for inhibition of HSA aggregation at 50 °C under stirring conditions. Below its thermal transition temperature, HSA is partially unfolded and provides optimum exposed side chains for favorable interactions of the exposed polar/ionic as well as hydrophobic side chains on protein molecules with these antioxidants. This optimum interaction brings about the inhibition of fibrillation efficiently (for example melatonin in this case). The TEM images also demonstrated that in presence of melatonin HSA aggregates size has reduced compared to either in the absence or in the presence of glutathione. The above studies not only demonstrate the mechanism of inhibition of HSA aggregation by melatonin but also quantify the inhibition ability in terms of heats of interactions  $(\Delta H_{lim}^0)$ . These results have implications for design of melatonin like drugs against HSA-aggregation prone diseases. Identification of the nature of interactions is a key step towards the discovery and synthesis of target oriented potential inhibitors and our data may help in designing lead molecules for development of potential therapeutic strategies.

## Acknowledgements

The authors are thankful to Indian Institute of Technology Bombay, Mumbai for providing HR-Transmission Electron Microscopic facility. Department of Science and Technology-Science and Engineering Research Board (DST-SERB), India (SB/FT/CS-169/2013), New Delhi is appreciatively acknowledged for financial assistance.

## References

1. R.M. Murphy, *Annu. Rev. Biomed. Eng.*, **2002**, 4,155-174.
2. D.P. Raleigh, *J. Phys. Chem. Lett.*, **2014**, 5,2012-2014.
3. C. Haass, D.J. Selkoe, *Nat. Rev. Mol. Cell Biol.*, **2007**, 8, 101-112.
4. M. Maheshari, S. Shekhar, B.K. Singh, I. Jamal, N. Vatsa, V. Kumar, A. Sharma, N.R. Jana, *Hum. Mol. Genet.*, **2014**, 23, 6235-6245.
5. C. A Ross, M.A. Poirier, *Nat. Med.*, **2004**, 10, S10-S17.
6. T. K. Chaudhuri, S. Paul, *FEBS J.*, **2006**, 273, 1331-1349.
7. M. Dasgupta and N. Kishore, *PLoS ONE.*, **2017**, 12(2), e0172208.
8. T. Peters Jr, *San Diego: Academic Press*, **1996**, 9-75.
9. M. Gabor, K. Fred, *J. Am. Chem. Soc.*, **1957**, 79, 134-139.
10. S. Sugio, A. Kashima, S. Mockizuki, M. Noda, K. Kobayashi, *Protein Eng.*, **1999**, 12, 439-446.
11. A.A. Bhattacharya, T. Grune, S. Curry, *J. Mol. Biol.*, **2000**, 303, 721-732.
12. A. Varshney, P. Sen, E. Ahmed, M. Rehan, N. Subbarao, *Chirality*, **2010**, 22, 77-87.

13. J. Gulam, P.A. Zunszain, I. Petipas, A.A. Bhattacharaya, M. Otagiri, S. Curry, *J. Mol. Biol.*, **2005**, 353, 38-52.
14. N. Zaidi, E. Ahmad, M. Rehan, G. Rabbani, M.R. Ajmal, Y. Zaidi, N. Subbarao, R.H. Khan, *J. Phys. Chem. B*, **2013**, 117, 2595-2604.
15. N.V. Bhagvan, C. E. Ha, *BBA Gen. Subject.*, **2013**, 12, 5486-5493.
16. P. Vorobey, A.E. Steindal, A. Vorobey, J. Moan, *J. Photochem. Photobiol.*, **2006**, 82, 817-822.
17. A. Stirpe, M. Pantusa, B. Rizzuti, L. Sportelli, R. Bartucci, R. Guzzi, *Int. J. Biol. Macromol.*, **2011**, 49, 337-342.
18. M. Bhattacharya, N. Jain, S. Mukhopadhyay, *J. Phys. Chem. B.*, **2011**, 115, 4195-4205.
19. P. Taboada, S. Barbosa, E. Castro, V. Mosquera, *J. Phys. Chem B.*, **2006**, 110, 20733-20736.
20. S. Matsushita, V.T. Chuang, M. Kanazawa, S. Tanase, K. Kawai, T. Maruyama, A. Suenaga, M. Otagiri, *Pharm. Res.*, **2006**, 23, 882-891.
21. N.K. Pandey, S. Ghosh, D.R. Tripathy, S. Dasgupta, *Protein Pept. Lett.*, **2015**, 22, 112-118.
22. N. Sharma, V. Sivalingam, S. Maurya, A. Prasad, P. Khandelwal, S.C. Yadav, B.K. Patel, *FEBS Letters.*, **2015**, 589, 4033-4038.
23. T. Arakawa, Y. Kita, *J Pharm Sci.*, **2000**, 89, 646-651.
24. S. Bag, R. Mitra, S. DasGupta, S. Dasgupta, *J. Phys. Chem. B .*, **2017**, 121, 5474-5482.
25. J.N. Abraham, D. Kedracki, E. Prado, C. Gourmel, P. Maroni, C. Nardin, *Biomacromolecules.*, **2014**, 15, 3253-3258.
26. K.C. Nadimpally, A. Paul, B. Mandal, *ACS Chem. Neurosci.*, **2014**, 5, 400-408.
27. B. Halliwell, J.M.C. Gutteridge, *Biochem. J.*, **1984**, 219,1-14.
28. G. Colombo, M. Clerici, D. Giustarini, R. Rossi, A. Milzani and I. Dalle-Donne, *Antioxid.Redox Signal.*, **2012**, 17, 1515-1527.
29. M.K. Siddiqi, P. Alam, S.K. Chaturvedi, R.H. Khan, *Int. J. Biol. Macromol.*, **2016**, 92, 1220-1228.
30. S. Awasthi, N.T. Saraswathi, *Int. J. Biol. Macromol.*, **2016**, 87, 1-6.
31. A.Stirpe, M.Pantusa, B.Rizzuti, M.P. De Santo, L.Sportelli, R.Bartucci, R.Guzzi, *Int. J. Biol. Macromol.*, **2016**, 92, 1049-1056.
32. T.Kar, P.Basak, R.K. Ghosh, M. Bhattacharyya, *Int. J. Biol. Macromol.*, **2017**, 99, 600-607.
33. V. Srinivasan, S.R. Pandi-Perumal, D.P. Cardinali, B. Poeggeler, R. Hardeland, *Behav.Brain.Funct.*, **2006**, 2, 15.
34. D.X. Tan, R. Hardeland, L.C. Manchester, A. Korkmaz, S. Ma, S. Rosales-Corral, R.J. Reiter, *J. Exp. Bot.*, **2012**, 63, 577-597.
35. J. J. Garcia, R.J. Reiter, J. M. Guerrero, G. Escamer, B.P. Yu, C.S. Ohand, A. Munoz-Hoyos, *FEBS Lett.*, **1997**, 408, 297-300.
36. S.R. Pandi-Perumal, A.S. BaHammam, G.M. Brown, D.W. Spence, V.K. Bharti, C. Kaur, R. Hardeland, D.P. Cardinali, *Neurotox. Res.*, **2013**, 23, 267-300.
37. M.I. Pablos, R.J. Reiter, J.I. Chuang, G.G. Ortiz, J.M. Guerrero, E. Sewerynek, M.T. Agapito, D. Meleghiorri, R. Lawrence, and S.M. Deneke, *J. Appl. Physiol.*, **1997**, 83, 354.
38. S.R. Pandi-Perumal, V. Srinivasan, D.W. Spence, D.P. Cardinali, *CNS Drugs.*, **2007**, 21, 995-1018.
39. K.J. Reid, P.C. Zee, *Semin Neurol.*, **2009**, 29, 393-405.
40. M. Kotlar, C. Rodriguez, R.M. Sainz, R. Antolin, A.M. Pelaez, *J Pineal Res*, **1998**, 24, 83-89.
41. A. Pompella, A. Visvikis, A. Paolicchi, V. Tata, A.F. Casini, *Biochem. Pharmacol.*, **2003**, 66, 1499-1503.
42. A. Pastorea, G. Federicia, E. Bertinib, F. Piemonteb, *Clin.Chim. Acta.*, **2003**, 333, 19-39.
43. O.W. Griffith, *Free Radic. Biol. Med.*, **1999**, 27, 922-935.
44. J. Chen, Z. He, H. Liu, C. Cha, *J. Electroanal. Chem.*, **2006**, 588, 324-330.
45. H. B. Noh, P. Chandra, J.O. Moon, Y.B. Shim, *Biomaterials.*, **2012**, 33, 2600-2607.
46. A. Pastore, F. Piemonte, M. Locatelli, R. Lo, L. Anna, L. M. Gaeta, G. Tozzi, G. Federici, *Clin. Chem.*, **2003**, 47, 1467-1469.
47. R.J. Reiter, R.C. Carneiro, C.S. Oh, *Horm. Metab. Res.*, **1997**, 29, 363-372.
48. M. Janiak, M. Suska, W. Dudzinska, E. Skotnicka, *J. Anim. Physiol. Anim. Nutr. (Berl.)*, **2010**, 94, 137-145.
49. B. Poeggeler, S.Saarela, R.J. Reiter, D.X. Tan, L.D. Chen, L.C. Manchester, L.R. Barlow-Walden, *Ann. N. Y. Acad. Sci.*, **1994**, 738, 419-420.
50. S.S. Pertsov, L.S. Kalinichenko, E.V. Koplík, L.G. Nagler, E.S. Alinkina, A.I. Kozachenko, *Biochem. Moscow Suppl. Ser. B*, **2014**, 8, 331-335.
51. R.J. Reiter, M.I. Pablos, T.T. Agapito, J. M. Guerrero, *Ann. N. Y. Acad. Sci.*, **1996**, 786, 362-378.
52. T. Chatterjee, A. Pal, S. Dey, B.K. Chatterjee, P. Chakrabarti, *PLoS One*, **2012**, 7(5), e37468.
53. J Wall, C.L. Murphy, A. Solomon, *Methods Enzymol.*, **1999**, 309, 204-217.
54. H. Levine, *Protein Sci.*, **1993**, 2, 404-410.
55. S.N. Save, S. Choudhary, *RSC Adv*, **2017**, 7, 20460-20468.
56. M. Ohi, Y. Li, Y. Cheng, T. Walz, *Biol. Proced. Online*, **2004**, 6, 23-34.
57. J. Juarez, P. Taboada, V. Mosquera, *Biophys. J.*, **2009**, 96, 2353-2370.
58. S. Chakraborty, R. Nandi, M. Maiti, *Biochem.Pharmacol*, **1990**, 39, 1181-1186.
59. A. Cooper, C. M. Johnson, *Methods Mol. Biol*, **1994**, 22, 109-124.

# Exploiting Materials to Design Novel Epigenetic Assays Towards Developing Algae for Screening Cancer Drugs

Subhojit Sen\*, Pooja Potdar and Patricia Pinto

UM-DAE Centre for Excellence in Basic Sciences (CEBS), Department of Biological Sciences,  
Mumbai University, Kalina Campus, Mumbai.

\*E-mail: subhojit.sen@cbs.ac.in

## Abstract

We are interested in how the environment dictates our susceptibility to cancer, by tracking plasticity of underlying epigenetic mechanisms. Using both mammalian as well unicellular models, we aim to decipher which epi-genetic signatures drive carcinogenesis. Using chromatin immunoprecipitation (ChIP), we demonstrated how three silencing pathways [DNA methylation, Polycomb (PRC2/4) and Histone Deacetylation (HDAC/SIRT1) come together upon oxidative damage, to silence tumour suppressor genes, thereby laying down a predisposition to cancer (O'Hagan *et al.*, 2011). To decipher how these faulty epigenetic memories are created in stem cell models, we used magnetic micro-beads to sequentially capture combinatorial histone modifications from human stem cell models, and mapped these mono-nucleosomes genome wide, to demonstrate an anti-correlation of bivalent-chromatin as well as H2A.Z (histone variant), to DNA methylation (Sen *et al.*, 2016). Having laid the foundation for these epigenetic memories in human models, we are establishing a unicellular green algae *Chlamydomonas*, which harbours genes from the three pathways, as a model to track conserved epigenetic mechanisms that can modulate transgene expression. Using agar based gradient-plate techniques we designed a novel epigenetic screen, which allows grouping of different pathways based on phenotype, allowing a simple screen to identify new epigenetically active compounds from indigenous medicinal and plant sources (Kaginkar *et al.*, submitted). In addition, using zirconia micro-bead abrasion, we devised novel strategies to generate nucleosomal ladders in *Chlamydomonas*, hitherto unachievable from cell wall plus wild type strains (D'Souza *et al.*, accepted). In summary, we are using materials both at the mega as well as micro scale, to develop novel assays to track epigenetic memories in model systems, which will aid in discovery of cancer epigenetic drugs.

## Introduction

Cancer is a disease of developmental programmes gone rogue leading to chaos, both at the genomic as well as proteomic level. Although cancer has genetic roots in the manifestation of "uncontrolled cell proliferation", it evolves from a complex interaction of the somatic milieu with its environment. In short, an onslaught of dietary, disease history, or behavioural (eg. smoking) insults that we are exposed to during our lifetime (or even trans-generationally), are carried forward as cellular memories, which later predispose us to varying degrees of injury, pushing normal cells towards becoming cancerous. How the environment changes us as genetic beings during our lifetimes, lies at the heart of epigenetic enquiry. Many genetic ailments (including cancer, Alzheimer's, diabetes, obesity etc.) that result from mutational loss of protein function, are mirrored by highly plastic epigenetic mechanisms that turn off gene expression, essentially mimicking genetic knock-outs. Understanding the evolutionary conservation of these epigenetic silencing modules that are altered

in cancer, will allow us to exploit cost-effective model systems to devise targeting technologies, that can be tested in humans as well.

## Epigenetic studies in Human systems:

Based on our previous studies, we hypothesize that DNA methylation, Polycomb mediated histone methylation and histone deacetylation, mediate gene silencing via CpG DNA methylation, which makes our genes susceptible to epigenetic change (O'Hagan *et al.*, 2011). Using magnetic microbeads (Dynabeads), we performed chromatin immunoprecipitation (ChIP) which enables us to query the associated epigenetic marks on respective genes. Using the oxidative stress paradigm, which itself has pleiotropic effects, we showed that DNA methyltransferases, PRC2 proteins and HDACs (SIRT1), come together to form a large silencing complex that actively shuts down gene transcription of the DNA damaged genes. However, after the damage is repaired and the system returns to homeostasis, some of these low expressing genes remain silenced and are eventually DNA methylated. Our analysis

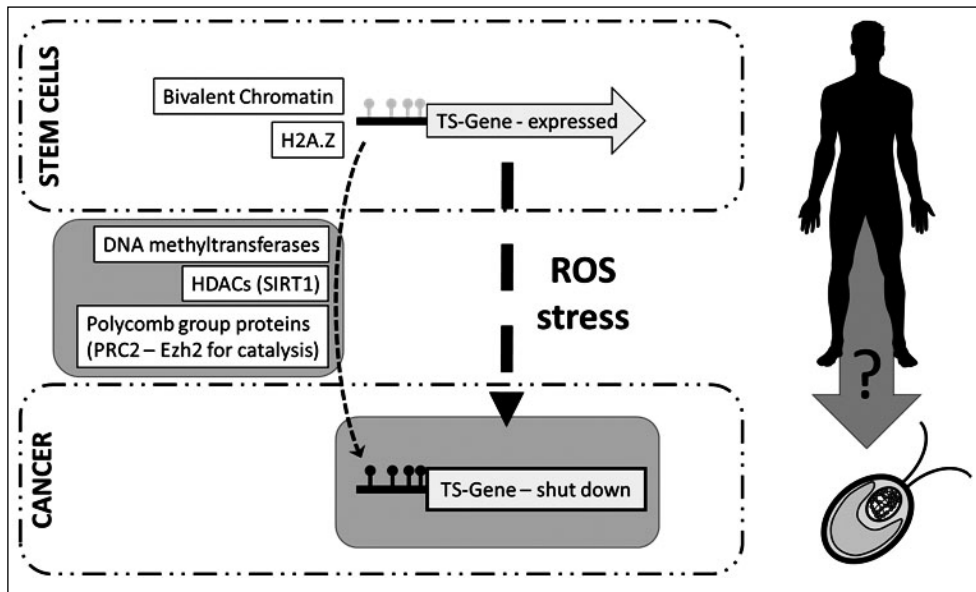


Figure 1: Epigenetic mechanisms of cancer – a query for conservation: A schematic representation of the ROS stress pathway, that eventually leads to silencing of tumour suppressor genes in humans, which leads to cancer. Our hypothesis states that bivalency and H2A.Z marked nucleosomes prevent the early onset of abnormal CpGDNA methylation of tumour suppressor (TS) genes (indicated by black lollipops), as a function of the ROS DNA damage pathway, which is mediated by a concerted interaction of DNMTs, HDACs and Polycomb proteins together. Our studies in the parallel unicellular algal model *Chlamydomonas* point to the fact that DNA methylation might drive transgene silencing in *Chlamydomonas*, which maintains sequence and structural conservation of all the above three pathways (conservations are highlighted by the grey boxes).

indicated that tumour suppressor genes are largely susceptible to this kind of shut down, thereby creating a fertile background for oncogenic mutations to now bypass the cellular surveillance pathways and lead to cancer (Fig 1). We also noticed that a significant portion of genes that are hypermethylated in cancer, seem to be bivalently marked in stem cells. However, mapping of bivalent marks genome wide has been a challenge.

Again, we used the magnetic microbeads to develop a modified sequential-ChIP which could capture and identify mononucleosomes harbouring both the H3K4me3 (active) and H3K27me3 (repressive) mark. Thus we were able to map and correlate mononucleosomes genome wide in a stem cell model, to show an antagonistic correlation between DNA methylation and two epigenetic marks, namely bivalent nucleosomes at the promoter and the histone variant, H2A.Z (Sen *et al.*, 2016). Together this points to a molecular barrier to cancer specific DNA methylation in stem cells, which if breached can eventually lead to faulty memories of the type we had earlier noticed in the oxidative stress paradigm (Fig 1).

### Epigenetic studies in *Chlamydomonas*:

The conservation of cancer specific methylation of gene promoters (CpG) to mediate silencing can

be traced down evolution to even unicellular eukaryotes like *Chlamydomonas* (Yamasaki *et al.*, 2008). Using both physical as well as chemical materials, we designed epigenetic assays that query how *Chlamydomonas* interacts with its environment to modulate gene expression. This allows us to biologically model the minimalist denominator of silencing pathways and abrogate them with drugs, and test them in humans (Xie *et al.*, 2017).

To track the above paradigm in *Chlamydomonas*, we designed a discovery screen that could potentially relate phenotype directly to epigenetic alterations (Kaginkar *et al.*, submitted). As proof of principle, using a DNA methylation inhibitor (cytosine analogue 5'-aza-2'-deoxycytidine, DAC) and molecular methylation assays (MSRE), we described how transgene silencing in

*Chlamydomonas* can be effected by DNA methylation (Fig 1). This “Epigenetic assay” allowed us to address, in one single assay step, not only the epigenetic activity of an unknown compound, but its possible mode of action as well. Using the assay, we developed a gradient plate methodology to identify new epigenetically active compounds, which could potentially hold promise in cancer therapy. Akin to phenotypes displayed by Sodium butyrate as a positive mediator, we identified Cinnamic acid as a potential deacetylation inhibitor (Kaginkar *et al.*, submitted). Curcumin on the other hand, displayed epigenetic activity that was clearly unlike the deacetylation phenotype. In two distinct steps, this growth-based assay tests for both initiation of epigenetic memory as well as transmission or maintenance across several generations. Exploiting this facet, we have been able to test combinatorial effects of epigenetic memory of one drug over another, in affecting gene silencing phenotypes. We have demonstrated how DAC can undo epigenetic effects mediated by pre-exposure to curcumin, implying its role in DNA methylation. This has major implications in understanding how combinatorial therapies might be useful in targeting cancer mechanisms in humans, since exposure to DAC is known to activate multiple pathways in tumours, which in turn makes them good candidates

for immunotherapy. Can pre-exposure to one epigenetic drug make cancerous cells more susceptible to other epigenetic compounds? We are currently developing this paradigm by using sequentially different combinatorial drug exposures, to address epigenetic gene silencing and co-relate it to activating tumour suppressor genes in human cell lines.

Although we have been successful in designing chemical intervention strategies to epigenetic mechanisms, Micrococcal Nuclease (MNase) digestion, the gold standard assay for epigenetic mapping has been impossible in *Chlamydomonas*, largely due to the presence of the cell wall. Nuclei isolation, a prerequisite for MNase digestion, has been possible only from cell wall minus (*cw*<sup>-</sup>) mutant strains (which are severely phenotypically compromised), making its applicability very limited. Removal of this thick cell wall is not only tedious but also uses harsh proteolytic enzymes which degrade the histones and damage the nuclei, rendering them relatively useless for epigenetic query. We therefore had to discover novel strategies to digest nuclear chromatin directly, by designing methodologies that would not only work in spite of the cell wall, but also circumvent nuclei isolation as well. We envisaged that agitating the cells in the presence of dense micro-bead materials could mechanically disrupt the cell wall, which in turn would make the cells immediately permeable to exogenously added MNase (D'Souza *et al.*, 2018). We abraded *cw*<sup>+</sup> wild type strains of *Chlamydomonas*, by vortexing them with 700  $\mu$ M zirconia beads or 600  $\mu$ M glass beads, in the presence of MNase. The addition of divalent ions (Ca<sup>+2</sup> and Mg<sup>+2</sup>) activated the nuclease while the reaction could be controlled and stopped by addition of EDTA as chelator. Using multiple standardizations and controlled conditions, we were successful in obtaining MNase derived nucleosomal ladders from *Chlamydomonas*, which could finally be used as chromatin substrates for mapping (Potdar *et al.*, *submitted*).

## Conclusions:

In summary, we conclude that we have successfully used hard materials (magnetic beads), soft (agar) gels, as well as soluble chemicals, to address physical as well as biological effects on epigenetic systems. Each has led us to uncover fundamentally conserved mechanisms in *Chlamydomonas* biology, a facet that reiterates its versatility as a model system, crucial to novel epigenetic strategies that might help us target cancer mechanisms in humans. Model systems as this will allow us to build cost-effective high-throughput screens for drug discovery, wherein we can screen indigenous plant and Ayurvedic sources for epigenetic compounds, not only useful in targeting multiple diseases but also in the betterment of our daily interaction with the environment.

## Acknowledgement:

We thank the Ramalingaswami Fellowship (DBT, India) for funding the study, and we thank all the previous members of the Sen lab at CEBS who have contributed to these studies over the years.

## References:

1. N. D'Souza, P. Joshi, S. Kaginkar, S. Sen. *Plant Molecular Biology Reporter*, **2018**, (in press). doi: doi.org/10.1007/s11105-018-1072-4.
2. O'Hagan, H. M., Wang W, Sen S *et al.*, *Cancer Cell*. **2011**, 20(5), 606-619.
3. P. Potdar, P. Pinto, N. D'Souza, P. Joshi, A. Malwade, S. Sen. *Protist*, 2018. '.
4. S. Sen, K.F. Block, A. Pasini, S. Baylin, H. Easwaran, *BMC Medical Genomics.*, **2016**, 9(1), 60.
5. S. Kaginkar, M. Jones, J. James, U. Sharma, J. S. D'Souza, S. Sen.', (*submitted*).
6. W. Xie, I. Kagiampakis, L. Pan, Y. W. Zhang, L. Murphy, Y. Tao, X. Kong, L. Xia, F. Carvlho, S. Sen, R-W Chiu Yen, C. A Zahnow, N. Ahuja, S. B. Baylin, *Cancer Cell*, **2017**.
7. T. Yamasaki, H. Miyasaka, T. Ohama, *Genetics*, 2008, 180(4), 1927-1944.



### **Subhojit Sen**

Current: Ramalingaswami Fellow, UM-DAE Centre for Excellence in Basic Sciences, Mumbai University, Kalina Campus, Santacruz (East), Mumbai 400098. Maharashtra, India.

Expertise: Molecular Biology, Epigenetics, Genetics, Biochemistry & Genomics.

Previous Background: 2007, Research Fellow, Johns Hopkins Medical Inst., JHU, Baltimore USA (with Prof. Stephen Baylin).

2002, Visiting Fellow, National Cancer Institute, National Institutes of Health (NIH) Bethesda, USA (with Prof. Carl Wu)

2001, Post-doctoral Fellow, TIFR, Mumbai, India.

2001, Ph.D. TIFR, Mumbai University, Mumbai, India (with Prof. B.J. Rao).

1996, M.Sc. Microbiology, M.S. University of Baroda, India (with Prof. B.B. Chattoo).

1994, B.Sc. Microbiology, Mumbai University, India

#### Honours:

Ramalingaswami Fellowship, DBT, India, Fogarty Research Fellowship, USA

Zita Lobo Memorial Award, TIFR, India.

J.N. Petit Memorial Award, Mumbai University, India.



### **Pooja Potdar**

Current: Junior Project Assistant (Biology), UM-DAE Centre for Excellence in Basic Sciences, Mumbai University, Kalina Campus, Santacruz (East), Mumbai 400098, Maharashtra, India.

Previous Background:

2013, M. Sc. Biotechnology, Symbiosis International University, Pune.

2011, B. Sc. Biotechnology, Bharati Vidyapeeth University, Pune.



### **Patricia Pinto**

Current: Research Associate-I (Biology), UM-DAE Centre for Excellence in Basic Sciences, Mumbai University, Kalina Campus, Santacruz (East), Mumbai 400098, Maharashtra, India.

Expertise: Molecular Biology, Immunology, Clinical Genetics, Haemostasis & Thrombosis.

Previous Background:

2010- 2014, Ph.D. Applied Biology, National Institute of ImmunoHaematology, (Indian Council of Medical Research), University of Mumbai (with Dr. Shrimati Shetty, Prof. Kanjaksha Ghosh).

2008-2009, Research Fellow, TIFR, Mumbai, Dept. of Biological Sciences (with Dr. Shobhona Sharma) 2008, M.Sc. Life Sciences (Applied Medical Sciences) St. Xavier's College, Mumbai. 2006, B.Sc. (Honours), Life Sciences & Biochemistry, St. Xavier's College, Mumbai.

#### Honours:

Developing World Scientist Award, awarded at the XXIII ISTH Congress & 57th Annual SSC Meeting, Kyoto, Japan.

Young Scientist Award, awarded at the International Conference of Human Genetics and 39th Annual ISHG Conference, India.

Best Paper Award, at the 55th Annual ISHTM Conference, India. Oral Papers, Laboratory (2nd Prize), at the 54th Annual ISHTM Conference, India.

Best Paper Award, at the 34th Annual MHG Conference, Mumbai, India.

Senior Research Fellowship, CSIR, India.

Lady Tata Memorial Trust Junior Scholarship for Scientific Research.

Invited Judge to Techno-Science Galaxy 2016, St. Andrew's College, Mumbai, India.

Novartis India Biotechnology Leadership Camp Team Winner 2016, India.

# Plasmonic modification of $\text{NaNbO}_3$ -CdS heterostructure photocatalyst for enhanced solar hydrogen generation

Kamala K. Nanda<sup>1</sup>, Hardik Jain<sup>1</sup>, Smrutirekha Swain<sup>1,2</sup> and Yatendra S. Chaudhary<sup>1,2,\*</sup>

<sup>1</sup>Colloids and Materials Chemistry Department, CSIR-Institute of Minerals and Materials Technology, Bhubaneswar-751 013, India

<sup>2</sup>Academy of Scientific and Innovative Research (CSIR-AcSIR), New Delhi, India

\*E-mail: yschaudhary@immt.res.in

## Abstract

The synthesized CdS- $\text{NaNbO}_3$  nanorod photocatalysts have been modified with plasmonic Au nanoparticles. The formation of phase pure CdS and  $\text{NaNbO}_3$  was confirmed by the X-ray diffraction, exhibiting the orthorhombic phase of  $\text{NaNbO}_3$  and hexagonal phase of CdS. The SEM analysis shows the formation of CdS- $\text{NaNbO}_3$  nanorods of high aspect ratio ( $40 \pm 5$  nm in width and  $1300 \pm 100$  nm in length). The anchoring of Au on the CdS- $\text{NaNbO}_3$  nanorods was confirmed by the presence of the plasmonic peak, as observed in the UV-Vis absorbance spectra. The CdS- $\text{NaNbO}_3$  nanorod photocatalyst shows the solar  $\text{H}_2$  generation rate of the order of  $54.21 \mu\text{molh}^{-1}$ , which enhances by more than two folds ( $118.37 \mu\text{molh}^{-1}$ ) upon modification of CdS- $\text{NaNbO}_3$  nanorod with Au nanoparticles. Such drastic enhancement is mainly because of the formation of Schottky junction between the Au nanoparticle and CdS- $\text{NaNbO}_3$  nanorods that facilitates improved separation of photogenerated charge carriers and thus improvement in the overall solar  $\text{H}_2$  generation rate.

## Introduction:

An enormous amount of untapped solar energy available can be directly converted to chemical energy ( $\text{H}_2$ ) by splitting water via photoelectrochemical/photocatalytic pathways. These pathways consist of three intriguing processes: (i) the harvesting of light that leads to the electron-hole pairs generation; (ii) the charge separation of photo-generated charge carriers and (iii) migration of photo-generated charge carriers to catalytic sites to drive fuel forming reactions. The photogenerated electrons drive the  $\text{H}^+$  reduction to  $\text{H}_2$  at reduction catalyst site and holes drive  $\text{H}_2\text{O}$  oxidation at oxidation catalyst site at which they are quenched by a reductant.<sup>1</sup> Ever since the report by Fujishima and Honda on photocatalytic water splitting using  $\text{TiO}_2$ , a variety of catalysts ranging from solid state, supramolecular and molecular catalysts coupled with light harvesters are being developed.<sup>2-11</sup> However, the desired efficiency and/or stability of these photocatalysts has not yet been achieved. It is mainly due to the mismatched energetics, poor control over recombination of photo-generated charge carriers and instability of catalysts and/or high overpotential requirements.

Plasmonic photocatalysis has drawn attention as one of the promising approaches to improve photocatalytic activity, in recent years.<sup>12-13</sup> It involves dispersal of noble metal nanoparticles (Au and Ag) into semiconductor photocatalysts. The plasmonic photocatalysis possesses two distinct features—a Schottky junction formation and localized surface plasmon resonance (LSPR); each benefits

photocatalysis differently. For instance, the Schottky junction formed at the contact of the noble metal and the semiconductor, builds up an internal electric field in a region (the space-charge region) close to the metal/semiconductor interface. This facilitates electrons and holes to move in different directions, once they are created in or near the Schottky junction. In addition, the metal provides a fast path for charge transfer and its surface acts as a charge-trap center to host more active sites for photoreactions. Secondly, the LSPR phenomenon renders the improvement in the light harvesting capability of photocatalysts. Third, the strong absorption causes most of the incident light to be absorbed in a thin layer ( $\sim 10$  nm) under the surface. Thus leading to a short distance between the photogenerated electrons and/or holes and the surface, which is comparable to the minority carrier diffusion length ( $\sim 10$  nm) and is beneficial for materials that show poor electron transport.

A class of metal oxide semiconductors possess layered structure and has drawn significant attention for their use as photocatalyst. Among many layered structure metal oxide materials  $\text{NaNbO}_3$  is a wide band gap semiconductor (3.3-3.4 eV), having perovskite structure and shows potential application for  $\text{H}_2$  generation.<sup>13-15</sup> However its wide band gap (3.3-3.4 eV can harvest only UV radiation) limit their applications. Herein, the  $\text{NaNbO}_3$  has been modified with CdS having the appropriate energetics, to ensure that it can harvest visible solar radiation. The CdS- $\text{NaNbO}_3$  heterostructures have further been modified with

plasmonic (Au) nanoparticles. The overall photocatalytic solar  $H_2$  generation activity and optical properties of these synthesized photocatalysts are presented in detail.

## Experimental Section:

### Synthesis of photocatalysts:

**Chemicals Used:** Niobium ethoxide (99.95%, Aldrich), Sodium hydroxide and ethylene glycol used were obtained from Merck. To synthesize cadmium sulfide, cadmium acetate and sulfur were obtained from Merck. Dodecyl amine was procured from Aldrich and used as a surface passivation agent. Gold Chloride salt (Chloroauric acid,  $HAuCl_4 \cdot 3H_2O$ ) with Mol.wt of 393.83 g/mol and a minimum assay of 49 % was purchased from FINAR reagents. Tri Sodium Citrate with 99.0 % assay and Sodium Borohydride with Mol.wt of 37.83 g/mol were obtained from Qualigens and Merck, respectively.

**Synthesis of nanostructured  $NaNbO_3$ :** To synthesize  $NaNbO_3$  nanorods, 0.5 g of  $Nb(OC_2H_5)_5$  was mixed with 10 mL of ethylene glycol and subsequently, 1 ml of 20 M NaOH was added drop-wise at  $40^\circ C$ . The reaction mixture

was allowed to stir for 1 h. It was then transferred into a teflon-lined autoclave and allowed to age at  $200^\circ C$  for 24 h. The product was recovered by centrifugation and washed with distilled water and ethanol. The obtained powder ( $NaNbO_3$ ) was then subjected to calcination at  $550^\circ C$  for 4 h.

**Modification of nanostructured  $NaNbO_3$  with CdS:** To grow CdS onto sodium niobate nanorods, the solution consisting 2 mmol  $Cd(CH_3COO)_2 \cdot 2H_2O$ , 2 mmol S powder and 10 mL dodecylamine was introduced into the teflon lined vessel containing reaction mixture for sodium niobate as mentioned above. Further the reaction steps were followed as mentioned in sodium niobate nanorod synthesis.

**Modification of CdS- $NaNbO_3$  heterostructured photocatalyst with Au nanoparticles:** The glasswares and magnetic pellets were cleaned using aqua-regia solution ( $HNO_3$  - HCl in the ratio of 1:3), dried and stored in a dessicator. 400  $\mu L$  of 25 mM stock solution of  $HAuCl_4 \cdot 3H_2O$  (Chloroauric acid) was added to 38.9 mL of Deionized water. The solution was stirred for 1 min followed by addition of 1 mL of 10 mM stock solution of trisodium citrate. 50 mg of as synthesized CdS- $NaNbO_3$  powder was added to this solution with continuous stirring (30 min). Subsequently, 300  $\mu L$  of freshly prepared 0.1 M Sodium Borohydride solution (ice cold) was added at once to the solution with vigorous stirring. Finally, the Au modified CdS- $NaNbO_3$  nanorods were recovered by centrifugation, and subsequently washed with Deionized water (4times) and dried in the oven at  $60^\circ C$ .

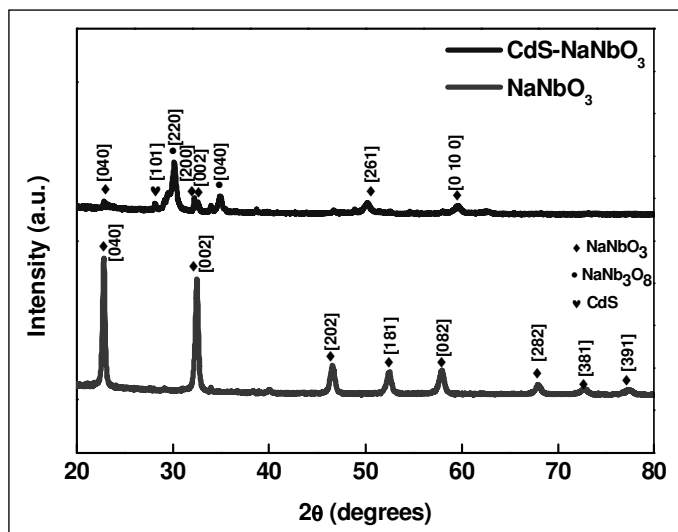


Figure 1. X-ray diffraction pattern of  $NaNbO_3$  and CdS- $NaNbO_3$

## Results and Discussion:

The synthesized samples were characterized with XRD to confirm their phase. The XRD pattern recorded for  $NaNbO_3$  exhibit the formation of orthorhombic phase of sodium niobate (Figure 1).

The grafting of CdS on  $NaNbO_3$  was confirmed by the appearance of the peak [101], corresponds to the hexagonal phase of CdS, as observed in addition to the peaks for the

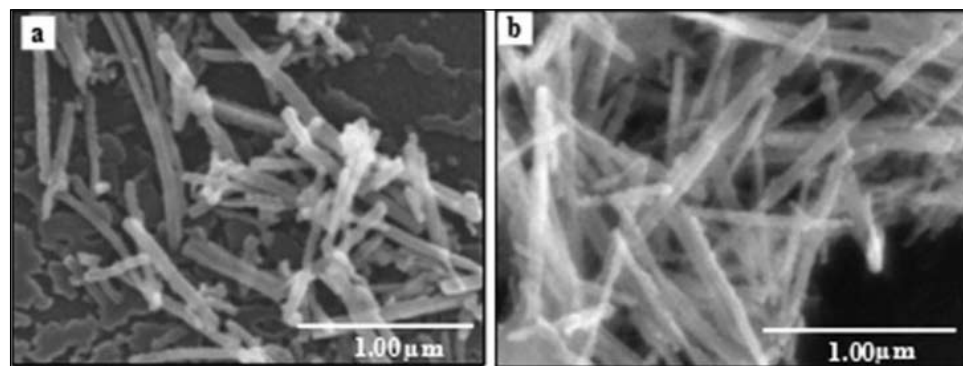


Figure 2. SEM image of (a)  $NaNbO_3$  and (b) CdS- $NaNbO_3$

orthorhombic phase of sodium niobate. The SEM images recorded for  $NaNbO_3$  and CdS- $NaNbO_3$  show the formation of nanorods (Figure 2). These nanorods are of the order of  $40 \pm 5$  nm in width and  $1300 \pm 100$  nm in length and have high aspect ratio.

The UV-Vis data show that CdS- $NaNbO_3$  nanorods absorb photons both in the UV and visible region. The UV absorption is due

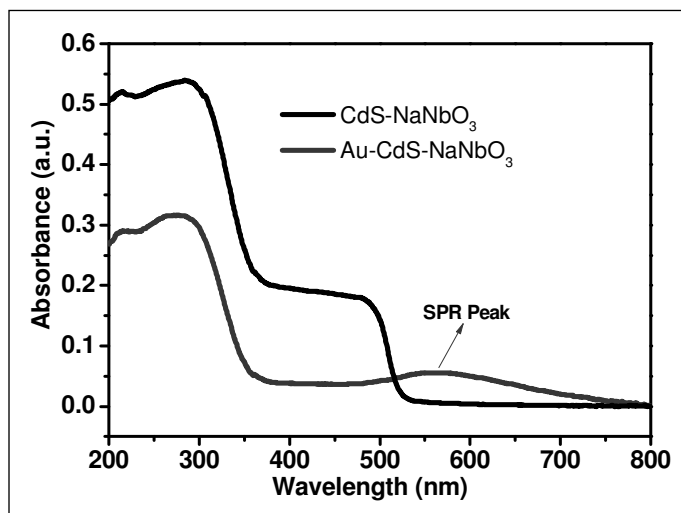


Figure 3. Absorbance spectra of CdS-NaNbO<sub>3</sub> and Au modified CdS-NaNbO<sub>3</sub>

to NaNbO<sub>3</sub> whereas the visible region absorption is due to the CdS. Upon modification of the CdS-NaNbO<sub>3</sub> nanorods with Au nanoparticles, the absorption in the visible region increased owing to the surface plasmon resonance of Au nanoparticles. The absorption edge exhibits a bathochromic shift due to localized surface plasmon resonance of Au nanoparticles, Figure 3.

The FTIR spectra recorded exhibit a peak at 3450 cm<sup>-1</sup>, which is due to the O-H stretching of the adsorbed water. This is further confirmed by the low intensity peak at 1649 cm<sup>-1</sup> which represents the absorption due to bending vibration of water. The absorbance in the region 520 to 840 cm<sup>-1</sup> is assigned to the stretching of Nb-O bond and further confirms the formation of NaNbO<sub>3</sub>. The FTIR spectra of Au modified CdS-NaNbO<sub>3</sub> has no

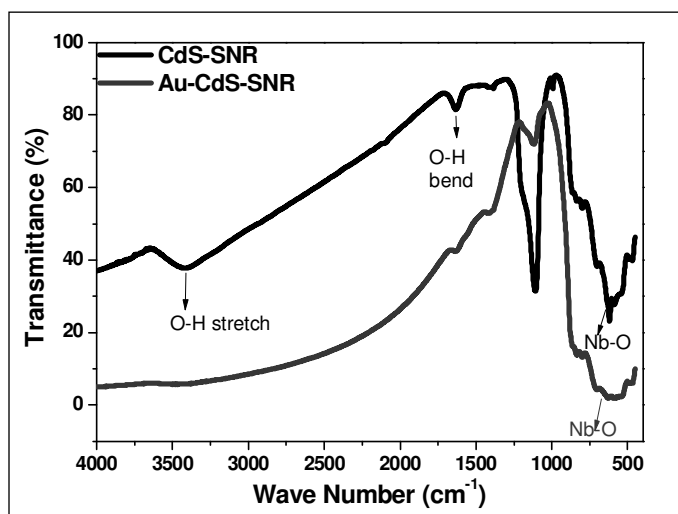


Figure 4. FTIR Spectra of CdS-NaNbO<sub>3</sub> and Au modified CdS-NaNbO<sub>3</sub>

extra peaks when compared to that of the spectra of CdS-NaNbO<sub>3</sub>, Figure 4, thus implying that there is no chemical bonding between Au nanoparticles and CdS-NaNbO<sub>3</sub> nanorods.

The photocatalytic hydrogen generation activities of CdS-NaNbO<sub>3</sub> nanorod powder and Au modified CdS-NaNbO<sub>3</sub> nanorod were measured under illumination using solar simulator (Hi-Tech) equipped with an AM 1.5G filter. The rate of hydrogen evolution using these photocatalysts is shown in Figure 5.

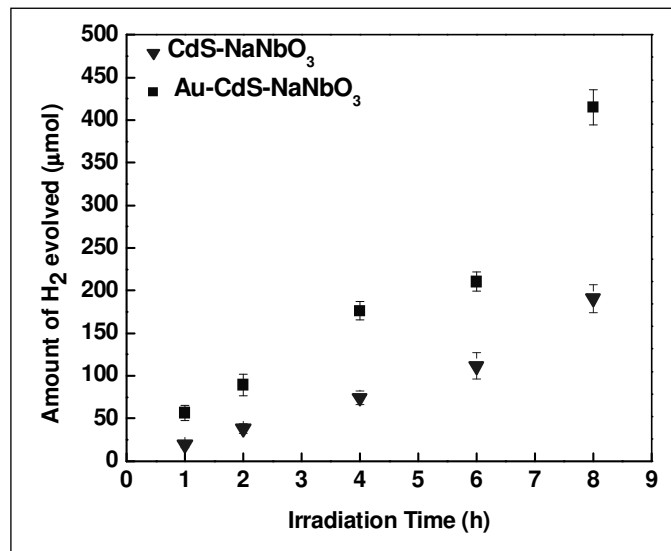


Figure 5. Solar H<sub>2</sub> generation as a function of time using CdS-NaNbO<sub>3</sub> and Au-CdS-NaNbO<sub>3</sub> photocatalysts; 10 mg photocatalyst, poly sulfide solution; 2.5 ml 0.1M Na<sub>2</sub>S and 0.14 M Na<sub>2</sub>SO<sub>3</sub>, pH ~ 12.4.

The CdS-NaNbO<sub>3</sub> nanorod photocatalyst exhibits the solar H<sub>2</sub> generation rate of the order of 54.21 μmol h<sup>-1</sup>. It further increases by more than two folds upon modification of CdS-NaNbO<sub>3</sub> nanorod photocatalyst with Au nanoparticles, and is of the order of 118.37 μmol h<sup>-1</sup>. Such drastic enhancement is mainly because of the formation of Schottky junction between the Au nanoparticle and CdS-NaNbO<sub>3</sub> nanorods, facilitating improved separation of photogenerated charge carriers and thus leading improvement in the overall solar H<sub>2</sub> generation rate.

## Conclusion:

In brief, the modification of the heterostructured CdS-NaNbO<sub>3</sub> nanorod photocatalyst with plasmonic (Au) nanoparticles enhances the photocatalytic hydrogen generation activity drastically. It is mainly due to the unified effect of the formation of a Schottky junction at CdS-NaNbO<sub>3</sub> nanorod-Au nanoparticle interface and localized surface plasmon resonance (LSPR). The Schottky junction pave the way for an efficient charge carrier separation at the Au-CdS-NaNbO<sub>3</sub> interface while LSPR enhances the

visible light absorption. These results serve an inspiration to design heterojunction photocatalysts based on plasmatic nanoparticle and photoactive semiconductors for improved solar H<sub>2</sub> generation. **Acknowledgement:** Authors are grateful to SERB (SB/FT/CS-023/2014) and MNRE (103/155/2009-NT), India for the financial assistance.

### References:

1. Y.S. Chaudhary, Solar Fuel Generation, CRC Press: Boca Raton, Florida, **2017**, 1-8.
2. A. Fujishima, K. Honda, *Nature*, **1972**, 238, 37.
3. T. W. Woolerton, S. Sheard, Y. S. Chaudhary, F. A. Armstrong, *Energy Environ. Sci.*, **2012**, 5, 7470.
4. M. Liu, N. L. Snapp, H. Park, *Chem. Sci.* **2011**, 2, 80.
5. K. Meyer, M. Ranocchiari, J.A. *Energy Environ. Sci.*, **2015**, 8, 1923.
6. Y. S. Chaudhary, T.W. Woolerton, C. S. Allen, J.H. Warner, E. Pierce, S. W. Ragsdale, F. A. Armstrong, *Chem. Commun.*, **2012**, 48, 58.
7. K. Maeda, K. Teramura, D. Lu, T. Takata, N. Saito, Y. Inoue, K. Domen, *Nature*, **2006**, 440, 295.
8. A. Bachmeier, V.C.C. Wang, T. W. Woolerton, S. Bell, J. C. Fontecilla-Camps, M. Can, S. W. Ragsdale, Y. S. Chaudhary, F.A. Armstrong, *Journal of the American Chemical Society*, **2013**, 135, 15026.
9. F. Lakadamyali, M. Kato, E. Reisner, *Faraday Discuss.*, **2012**, 155, 191.
10. R.V. D. Krol, Y. Liang and J. Schoonman, *J. Mater. Chem.*, **2008**, 18, 2311.
11. H. Zhou, Y. Qu, T. Zeid and X. Duan, *Towards Energy Environ. Sci.*, **2012**, 5, 6732.
12. X. Zhang, Y.L. Chen, R.S. Liu, D.P. Tsai, *Reports Prog. Phys.*, **2013**, 76, 046401
13. S.C. Warren, E. Thimsen, *Energy Environ. Sci.*, **2012**, 5, 5133.
14. K. Saito, A. Kudo. *Inorg. Chem.*, **2010**, 49, 2017.
15. H. Shi, X. Li, D. Wang, Y. Yuan, Z. Zou and J. Ye, *NaNbO<sub>3</sub> Catal. Lett.*, **2009**, 132, 205.

	<p><b>Kamala Kanta Nanda</b> received his B.Sc. degree in chemistry in 2007, and M.Sc. degree in Chemistry in 2009 from Utkal University, India. He earned Ph.D. degree while working extensively on photocatalytic H<sub>2</sub> Generation in Dr. Chaudhary's research group at CSIR- Institute of Minerals and Materials Technology, India. He is currently postdoctoral fellow (NPDF) at Indian Institute of Science, Bangalore. His research interests include: synthesis of nanostructured hetero-junction photocatalyst and their application in solar fuel generation.</p>
	<p><b>Hardik Jain</b> graduated from SRM University in 2015 with a B. Tech. degree in Nanotechnology and carried out research project at the CSIR-IMMT, Bhubaneswar, India. He moved to France to pursue an Erasmus Mundus Master's program in Materials Science during which he was fully funded by his prestigious Erasmus Mundus Scholarship. He has been recently offered a Marie Curie PhD fellowship at Holst Center, Netherlands and would be joining soon. His research proclivities mainly include thin film science, semiconductors, electronics and memory storage.</p>
	<p><b>Smrutirekha Swain</b> received her M.Sc. degree in Physics from National Institute of Technology, Rourkela in 2010. As a doctoral student at CSIR-IMMT her research work is focused on the identification of inexpensive and abundantly available metal based semiconducting photocatalysts to drive water splitting using visible light. In addition, she is also exploring their opto-electronic properties etc. in detail.</p>
	<p><b>Dr. Yatendra S. Chaudhary</b> is Senior Scientist at CSIR-Institute of Minerals &amp; Materials Technology, Bhubaneswar, India. He designed enzyme-semiconductor based photocatalysts for visible light driven CO<sub>2</sub> reduction and H<sub>2</sub> production while working at University of Oxford, UK. His research accomplishments have brought him many recognitions such as Green Talent-2011 Award from the BMBF, Germany, CSIR-Young Scientist Award-2013 from the CSIR, India and prestigious Marie Curie Fellowship by the European Union. He has edited a book -"Solar Fuel Generation" 1<sup>st</sup> ed. New York: CRC Press Taylor &amp; Francis Group, 2017. The research activities in his group are focused on various facets of nanomaterials and materials chemistry for solar fuel generation.</p>

**SOCIETY FOR MATERIALS CHEMISTRY (SMC)**  
(Reg. No. - Maharashtra, Mumbai/1229/2008/GBBSD)  
c/o Chemistry Division  
Bhabha Atomic Research Centre, Mumbai 400 085

**APPLICATION FOR MEMBERSHIP**

Please enroll me as a Life member of the *Society for Materials Chemistry (SMC)*. My particulars are as follows:

Name : \_\_\_\_\_

Educational Qualifications : \_\_\_\_\_

Field of Specialization : \_\_\_\_\_

Official Address : \_\_\_\_\_

Telephone No. (Off.) : \_\_\_\_\_

Residential Address : \_\_\_\_\_

Telephone No. (Res.) : \_\_\_\_\_

Address for Correspondence : Home/Office (Please tick one of the options)

E-mail Address : \_\_\_\_\_

-----  
Subscription Details

Mode of Payment : Cheque/DD/Cash  
(Cheque/DD should be drawn in favor of "*Society for Materials Chemistry*" for Rs. 1000/- payable at Mumbai. For out-station *non-multi-city* cheques, please include Rs.50/- as additional charge for bank clearance.

Number :

Dated :

Drawn on Bank & Branch :

Amount :

Place:

Date:

Signature

Registration Number: \_\_\_\_\_ (To be allotted by SMC office)





**AlfaTech Services**

# DRON-8

## X-ray multifunctional diffractometer

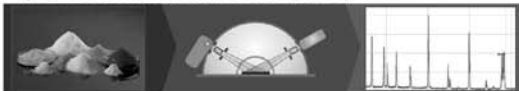
- High-precision wide-angle vertical theta-theta goniometer with changeable radius
- Automated alignment of sample plane
- Flexible configuration of X-ray optical scheme
- Wide range of options



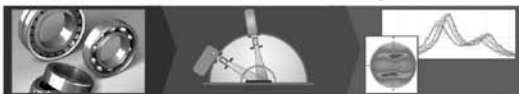
ALROSA GROUP  
RESEARCH AND PRODUCTION ENTERPRISE  
**BOUREVESTNIK**  
RESEARCH + DESIGN + PRODUCTION

### Application fields

#### Powder XRD (reflection, transmission, GID)



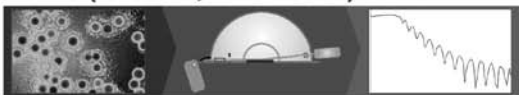
#### Texture and residual stress analysis



#### HR-XRD



#### SAXS (reflection, transmission) and XRR



### Advanced options

#### Multidrive attachments



#### X-ray optical elements



#### Registration systems





**PARTECH SCIENTIFIC INSTRUMENTS**  
214 2<sup>nd</sup> Floor , Arcadia ,Hiranandani Estate  
Patlipada, Thane (W) – 400607  
Tel No.: +91-86551 97444 / +91-22497 48855  
E-mail : [info@partech.co.in](mailto:info@partech.co.in)  
URL: [www.partech.co.in](http://www.partech.co.in)

## **ABOUT US**

**Partech Scientific Instruments** incorporated in year 2013, is a leading scientific instrument Sales, Marketing and Service company. We are Indian distributor of Hiden Isochema - UK, Altamira Instruments -USA, Porometer-NV - Belgium, CAD-Instruments – France, Occhio-France and LabDex-UK.

The Product Range includes,

### **A)Hiden Isochema – UK:**

- ✚ Fully automated gravimetric and manometric instruments
- ✚ dynamic vapor sorption (DVS) analyzers
- ✚ dedicated breakthrough analyzers
- ✚ climate control systems

### **B)Altamira Instruments – USA**

- ✚ Catalyst characterization - TPD, TPR, TPO, pulse chemisorption analyser
- ✚ Bench-scale, rack-mounted, catalytic micro-reactor systems from the BenchCAT line
- ✚ High throughput reactor systems for catalyst screening from the BenchCAT-HTS family
- ✚ Benchtop micro-reactor systems from the  $\mu$ BenchCAT line

### **C)Porometer-NV -Belgium**

- ✚ Characterization of porous membranes and filters
- ✚ Characterisation of nonwovens,
- ✚ Characterisation of ceramics, adsorbents, rocks

### **D)CAD – Instruments-France**

- ✚ Surface area and poresize analyser
- ✚ Gas Pycnometer
- ✚ Nano Particle size , Zeta Potential Analysers
- ✚ Rheometers for mortar and concrete

### **E)Ochhio – Belgium**

- ✚ Particle size with shape analysis
- ✚ Dry applications from 0.2 $\mu$ m to 3000 $\mu$ m
- ✚ Wet applications from 0.8 to 300 $\mu$ m

### **F)LabDex -UK**

LabDex product range of laboratory equipment includes Autoclaves, UV-VIS Spectrophotometers, Incubators, Laboratory Shakers, Furnaces, Homogenizers, Magnetic Stirrers, Hot Plates and Sample concentrators.

### **For more detail please contact us:**

Email : [pankajkadam@partech.co.in](mailto:pankajkadam@partech.co.in) / [keshabmaikup@partech.co.in](mailto:keshabmaikup@partech.co.in)



# ONGC ENERGY CENTRE

## SHAPING THE SUSTAINABLE FUTURE

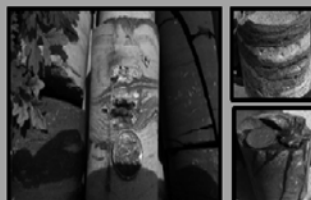
ONGC Energy Centre (OEC) functions under the aegis of the ONGC Energy Centre Trust (OECT), which was set up by Oil and Natural Gas Corporation Ltd (ONGC), with a mandate to undertake and/or assist/collaborate in research for developing and/or improving the technology options, applications, viable energy mediums and sources, especially in clean and renewable energy options which have the potential to make an impact on India's energy scene.

**Vision:** "Harness science and technology to meet national energy needs of tomorrow, in a clean and sustainable manner..."

OEC is engaged in In-house research, through own scientists/research teams as well as collaborative projects jointly taken up with some of the leading national academic and research institutions since 2007. The current broad areas of research pursued by OEC include (i) **Sub-surface Uranium exploration and recovery by in-situ leaching process**, (ii) **Hydrogen Energy**, (iii) **Biotechnology for Energy**, (iv) **Solar Energy**, (v) **Geothermal Energy** and (vi) **Energy Recovery /storage and others**.



Cu-Cl Closed Loop setup for Hydrogen generation – ICT, Mumbai



Sub-Surface Cores



CBM well Stimulation

### Highlights:

#### Technology / Process developed so far:

- Indigenous Process and Integrated facility /Equipment for Closed Loop Cu-Cl Cycle for Hydrogen generation.
- Indigenous process and equipment for I-S cycle for Hydrogen generation.
- Indigenous Polymeric Membranes
- Microbial bio-conversion process for Lignite to Methane and Humic Acid
- Microbial Process to enhance Gas Production in CBM wells
- Molten Salt Heat Storage Materials (120 °C – 750 °C)

#### Technology / Process under development:

- 2 MWe Concentrating Solar Thermal Power Plant based on Beam Down Technology
- Microbial Process to reduce SRBs and prevent souring and corrosion in oil field
- ISL process for extraction of sub-surface Uranium; 5 regions identified by exploration.
- Solar thermal dish Stirling engine systems
- Assessment & potential for Geothermal power in sedimentary regions

#### Infrastructure and IPR

- R&D facilities for Hydrogen, Uranium and Bio-technology
- 14 Patents filed relating to Hydrogen, Bio-technology and Solar Thermal, 3 Patents granted Internationally in several countries

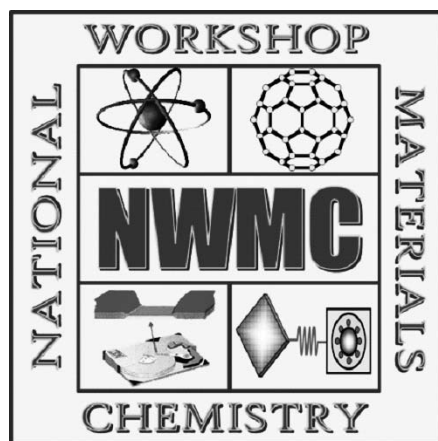
Office: 8<sup>th</sup> Floor, Core-3&4, SCOPE Minar, Laxmi Nagar, Delhi-110 092  
Phone - 011-2240 6089/6040/6036; Fax-22011783

[www.ongcindia.com/wps/wcm/connect/ongcindia/home/ongc-energy-centre](http://www.ongcindia.com/wps/wcm/connect/ongcindia/home/ongc-energy-centre)  
E-mail: [ongcenergycentre@ongc.co.in](mailto:ongcenergycentre@ongc.co.in)



MANIPAL UNIVERSITY  
JAIPUR

**5<sup>TH</sup> NATIONAL WORKSHOP  
ON MATERIALS CHEMISTRY  
(NANO & COMPOSITE MATERIALS)  
NWMC – 2019 (NCom-Mat)**



**November 7-8, 2019**

*Venue*

Manipal University Jaipur  
Jaipur-Ajmer Expressway, Jaipur, Rajasthan 303007

*Organized By*

Society for Materials Chemistry (SMC)  
C/o Chemistry Division, BARC, Mumbai - 400085  
&

Department of Chemistry  
School of Basic Sciences  
Manipal University Jaipur, Rajasthan 303007

For details please visit [www.smcindia.org](http://www.smcindia.org)  
contact: Dr. Lalita Ledwani  
Professor of Chemistry  
Director, School of Basic Sciences  
Email: [lalita.ledwani@jaipur.manipal.edu](mailto:lalita.ledwani@jaipur.manipal.edu)





*Printed by:*

**Ebenezer Printing House**

Unit No. 5 & 11, 2nd Floor, Hind Service Industries

Veer Savarkar Marg, Shivaji Park Sea-Face, Dadar (W), Mumbai - 400 028

Tel.: 2446 2632 / 2446 3872 Tel Fax: 2444 9765 E-mail: [outworkeph@gmail.com](mailto:outworkeph@gmail.com)

## In this issue

	Feature article	Page No.
1	<b>Fluorescent nanoaggregates through molecular self-assembly: morphology control and spectroscopic investigation</b> <i>MD. Waseem Hussain and Abhijit Patra</i>	1
2	<b>Influence of particle size of albumin nanoparticles on its drug loading and cellular uptake</b> <i>Beena G. Singh, Ram P. Das, Amit Kunwar</i>	8
3	<b>Effect of Zinc Oxide Nanoparticles on dc Electrical Conductivity of Inorganic-Organic Conducting Nanocomposites</b> <i>Shahid Pervez Ansari and Faiz Mohammad</i>	13
4	<b>Strategic design of gold nanoparticles for the complete elimination of tumour cells: Potential and challenges</b> <i>Manu Lopus</i>	20
5	<b>Effects of antioxidants melatonin and glutathione on human serum albumin aggregation: biophysical studies</b> <i>Vikas Kumar, Ramakrishna V. Hosur and Sinjan Choudhary</i>	22
6	<b>Exploiting Materials to Design Novel Epigenetic Assays Towards Developing Algae for Screening Cancer Drugs</b> <i>Subhojit Sen, Pooja Potdar and Patricia Pinto</i>	29
7	<b>Plasmonic modification of NaNbO<sub>3</sub>-CdS heterostructure photocatalyst for enhanced solar hydrogen generation</b> <i>Kamala K. Nanda, Hardik Jain, Smrutirekha Swain and Yatendra S. Chaudhary</i>	33

Published by  
**Society for Materials Chemistry**  
C/o. Chemistry Division  
Bhabha Atomic Research Centre, Trombay, Mumbai 40085  
e-mail: socmatchem@gmail.com, Tel: 91-22-25592001